Research Paper

Inadequate control of thyroid hormones sensitizes to hepatocarcinogenesis and unhealthy aging

Livia López-Noriega[1], Vivian Capilla-González[1], Nadia Cobo-Vuilleumier[1], Eugenia Martin-Vazquez[1], Petra Isabel Lorenzo[1], Enrique Martinez-Force[2], Mario Soriano-Navarro[3], María García-Fernández[4], Silvana Yanina Romero-Zerbo[5,6], Francisco Javier Bermúdez-Silva[5,6], Irene Díaz-Contreras[1,6], Ana Sánchez-Cuesta[7], Carlos Santos-Ocaña[7], Abdelkrim Hmadcha[1,6], Bernat Soria[6,8], Franz Martín[1,6], Benoit Raymond Gauthier[1,6], Alejandro Martin-Montalvo[1]

[1]Department of Regeneration and Cell Therapy, Andalusian Center for Molecular Biology and Regenerative Medicine-CABIMER, Junta de Andalucia-University of Pablo de Olavide-University of Seville-CSIC, Sevilla, Spain
[2]Instituto de la Grasa (CSIC), Universidad Pablo de Olavide, Sevilla, Spain
[3]Centro de Investigación Príncipe Felipe, Valencia, Spain
[4]Department of Human Physiology, Málaga University, Biomedical Research Institute of Málaga (IBIMA), Málaga, Spain
[5]Instituto de Investigación Biomédica de Málaga-IBIMA, UGC Endocrinología y Nutrición. Hospital Regional Universitario de Málaga, Málaga, Spain
[6]Biomedical Research Network on Diabetes and Related Metabolic Diseases-CIBERDEM, Instituto de Salud Carlos III, Madrid, Spain
[7]Centro Andaluz de Biología del Desarrollo, Universidad Pablo de Olavide and CIBERER, Sevilla, Spain
[8]Deptartment of Physiology, University Miguel Hernández School of Medicine Sant Joan d'Alacant, Alicante, Spain

Correspondence to: Alejandro Martin-Montalvo, Benoit Raymond Gauthier; **email:** alejandro.martinmontalvo@cabimer.es, benoit.gauthier@cabimer.es
Keywords: lifespan, healthspan, thyroid hormones, hyperthyroidism, hypothyroidism, glucose metabolism
Received: August 13, 2019 **Accepted:** September 5, 2019 **Published:** September 13, 2019

ABSTRACT

An inverse correlation between thyroid hormone levels and longevity has been reported in several species and reduced thyroid hormone levels have been proposed as a biomarker for healthy aging and metabolic fitness. However, hypothyroidism is a medical condition associated with compromised health and reduced life expectancy. Herein, we show, using wild-type and the Pax8 ablated model of hypothyroidism in mice, that hyperthyroidism and severe hypothyroidism are associated with an overall unhealthy status and shorter lifespan. Mild hypothyroid Pax8 +/- mice were heavier and displayed insulin resistance, hepatic steatosis and increased prevalence of liver cancer yet had normal lifespan. These pathophysiological conditions were precipitated by hepatic mitochondrial dysfunction and oxidative damage accumulation. These findings indicate that individuals carrying mutations on PAX8 may be susceptible to develop liver cancer and/or diabetes and raise concerns regarding the development of interventions aiming to modulate thyroid hormones to promote healthy aging or lifespan in mammals.

INTRODUCTION

The increasing burden of age-related diseases highlights the importance of uncovering the mechanisms underlying the aging process. Studies in animal models have identified several endocrine and metabolic factors that interact with aging pathways, including insulin, growth hormone (GH), insulin-like growth factor 1 and

thyroid hormone (TH) signalling among others [1–3]. The main THs produced in the thyroid gland are triiodothyronine (T3) and thyroxin (T4). In humans, 80% of the THs secreted by the thyroid gland is T4 and 20% is T3. T4 is converted by deiodinases into T3 within cells. TH secretion is tightly regulated under physiological conditions by the hypothalamus-pituitary-thyroid (HPT)-axis. The hypothalamus secretes thyrotropin-releasing hormone (TRH) that induces the transcription of genes required to generate and secrete the thyroid-stimulating hormone (TSH) in the hypophysis. TSH stimulates the production of T4 and T3 in the thyroid gland, which in turn inhibit both TRH and TSH synthesis when THs reach the hypothalamus and the hypophysis, respectively. THs in circulation reach the majority of somatic cells, *via* TH receptors, and modulate the expression of more than 80 genes, such as uncoupling proteins (UCPs), which ultimately produce an increase on the basal metabolic rate [4].

Greater life expectancy has been associated with reduced circulating levels of T4, T3, and/or high TSH levels in both, animal models and humans [3, 5–8]. In this line, the Laron (GH Receptor Knock Out; Ghr KO), Ames (Prop1-mutated) and Snell (Pit1-mutated) dwarf mice, which have reduced GH signalling and reduced circulating TH levels, exhibit a consistent exceptional lifespan as well as other metabolic alterations such as enhanced hepatic insulin sensitivity [9–12]. Both, rodents and humans under calorie restriction (CR), which comprises a variety of nutritional interventions with several beneficial effects including extended longevity, exhibit reduced circulating T3 levels and/or high TSH levels [13–15]. Interestingly, CR mimetics such as resveratrol alter the HPT axis (*e.g.* elevating TSH levels), suggesting that the modulation of THs might contribute to the beneficial effects conferred by these interventions [16].

Studies in humans have revealed that centenarians and their offspring display higher TSH levels in blood [17]. Likewise, nonagenarians from families with exceptional long lifespans, as well as their descendants, have been reported to exhibit increased TSH levels and/or decreased circulating T3 levels [18, 19]. Actually, mildly down-regulated thyroid function has been suggested to correlate with better function in old age and it has been proposed as a biomarker of healthy aging [18, 20, 21].

Several reports indicate that THs induce reactive oxygen species (ROS) production and oxidative stress, which could provide a causal link with aging [22–24]. However, THs have been shown to promote mitophagy and upregulate the expression of *Ucp2*, which might reduce ROS production [25–27]. In addition, epidemiological observations have indicated that, both hypothyroidism and subclinical hypothyroidism, are serious medical conditions associated with cardiovascular problems and several metabolic disorders, such as steatosis and cancer, that reduce health and increase mortality risk [28–31].

These contradictory observations led us to assess the specific effect of the modulation of TH levels in murine healthspan and lifespan using the Pax8 knock-out animal model of hypothyroidism (Wild type [Wt], Pax8 +/- and Pax8 -/-) supplemented or not with THs.

RESULTS

High or low TH levels compromise murine healthspan and lifespan

In order to determine the effect of lower levels of THs in mouse healthspan and lifespan, we used the murine Pax8 model of hypothyroidism [32]. In adulthood, *Pax8* is predominantly expressed in kidney and thyroid, while absent in several metabolic tissues (Supplementary Figure 1A). Pax8 -/- mice at 21 days of age were almost devoid of *Pax8* expression in the thyroid as well as circulating T4 levels, while maintaining normal α-glycoprotein subunit (α-GSU) levels of gonadotropic hormones when compared to Wt mice (Figure 1A and Supplementary Figure 1B–1C). Pax8 -/- mice displayed lower body and tissue weights, reduced food intake and hypoglycemia that result in peri-weaning death ($\chi^2 \geq 100$ and $P < 0.0001$ vs. Wt) (Figure 1B–1D and Supplementary Figure 1D–1G). *Pax8* expression in the thyroid as well as circulating T4 levels at weaning (21 days) were similar in Pax8 +/- mice when compared to Wt mice, whereas α-GSU was increased (Figure 1A and Supplementary Figure 1B–1C). As such, energy intake as well as body, organ weights and glycaemia were similar at 21 days of life in Wt and Pax8 +/- mice (Figure 1C–1D and Supplementary Figure 1D–1G). However, by the age of 8 months, *Pax8* expression was decreased in Pax8 +/- mice when compared to Wt mice, resulting in a mild but significant reduction in T4 circulating levels, an effect maintained for up to 24 months (Figure 1E–1F and Supplementary Figure 1H). Levels of α-GSU were similar to Wt levels at these time points (Supplementary Figure 1I–1J). Lower circulating T4 levels correlated with increased body weight in Pax8 +/- mice as compared to Wt mice (Figure 1G). Although not significant, Pax8 +/- mice showed a trend towards a shorter life expectancy when compared to Wt mice (Figure 1B). Necropsy revealed that Pax8 +/- mice were susceptible to develop with age liver cancers with hallmarks of hepatocellular carcinoma, as no gross anatomical alterations were detected at day 21 of life (Figure 1H–1I, Supplementary Figure 1K and

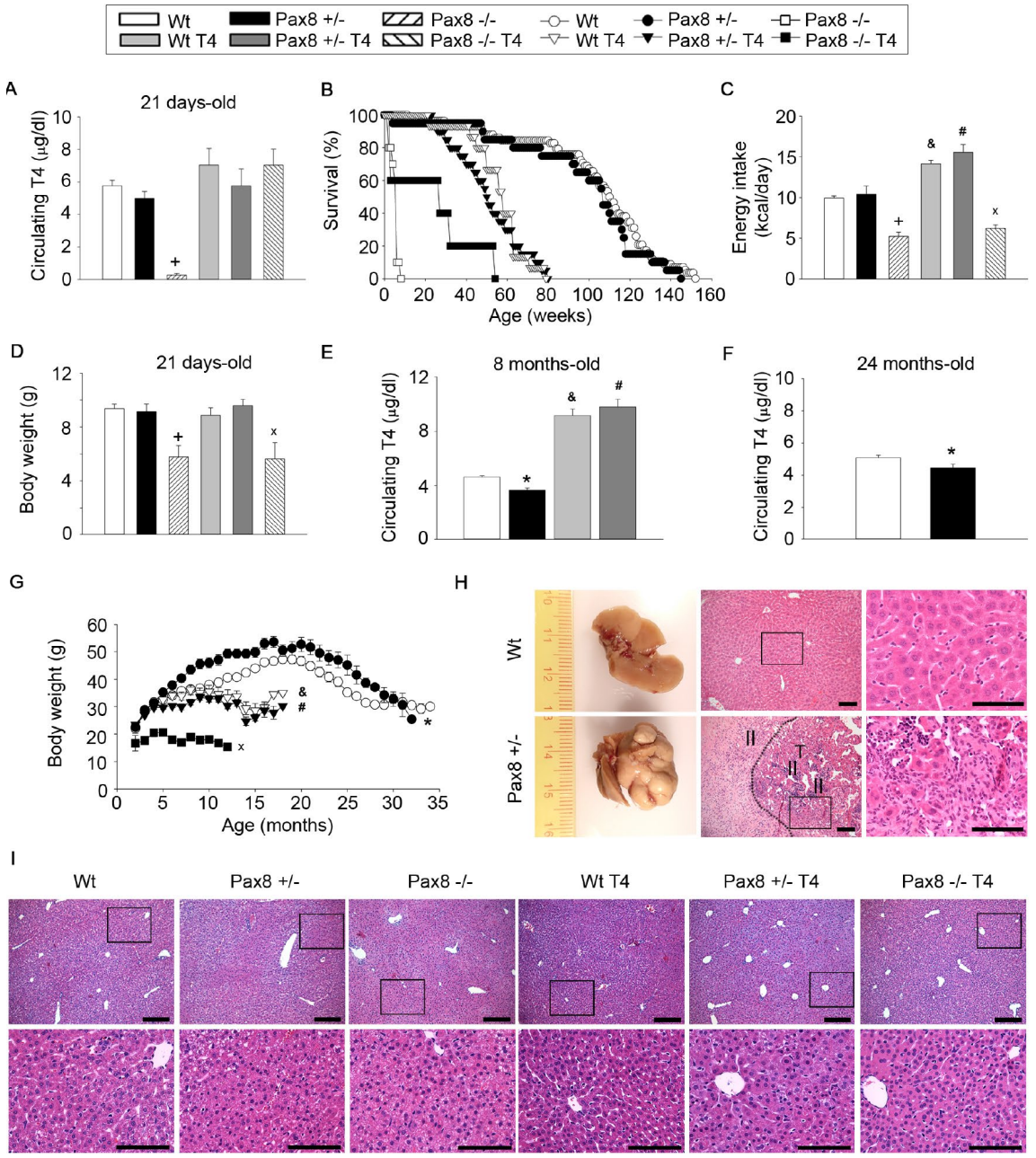

Figure 1. High or low TH levels compromise murine healthspan and lifespan. (**A**) Circulating T4 levels at 21 days of age. n = 5 Wt, n = 5 Pax8 +/-, n = 5 Pax8 -/-, n = 5 Wt T4, n = 5 Pax8 +/- T4, n = 3 Pax8 -/- T4. Two-way ANOVA. (**B**) Kaplan-Meier survival curve. n = 58 Wt, n = 20 Pax8 +/-, n = 10 Pax8 -/-, n = 15 Wt T4, n = 20 Pax8 +/- T4, n = 5 Pax8 -/- T4. Survival log rank test. (**C**) Basal daily energy intake in 5-weeks old mice. n = 5 Wt, n = 4 Pax8 +/-, n = 3 Pax8 -/-, n= 3 Wt T4, n = 3 Pax8 +/- T4, n = 3 Pax8 -/- T4 (the "n" reflects the number of cages). Two-way ANOVA. (**D**) Body weight at 21 days of age. n = 21 Wt, n = 15 Pax8 +/-, n = 5 Pax8 -/-, n = 11 Wt T4, n = 11 Pax8 +/- T4, n = 4 Pax8 -/- T4. Two-way ANOVA. (**E**) Circulating T4 levels at 8 months of age. n = 11 Wt, n = 5 Pax8 +/-, n = 7 Wt T4, n = 5 Pax8 +/- T4. Two-way ANOVA. (**F**) Circulating T4 levels at 24 months of age. n = 8 per group. T-test two tailed. (**G**) Body weight during longevity assay. n = all available mice of longevity assay (panel B). One-way ANOVA or ANOVA on ranks if distribution is not normal. * on months 6-17 and 21-28. & on months 12-18. # on months 3, 5-8 and 10-18. x on months 3-12. (**H**) Representative photographs and hematoxylin and eosin staining of liver tissue from Wt and Pax8 +/- mice at necropsies. Wt liver exhibits normal hepatic parenchyma with acinar architecture. Pax8 +/- liver displays primary liver epithelial neoplasms (T) with disorganized architecture and inflammatory infiltrate (II). Scale bar 100 um. n = 4 per group. See also Supplementary Figure 1K. (**I**) Histological analysis of liver tissue by hematoxylin and eosin staining at 21 days of age. n = 4 Wt, n = 5 Pax8 +/-, n = 5 Pax8 -/-, n = 5 Wt T4, n = 5 Pax8 +/- T4, n = 3 Pax8 -/- T4. Scale bars; top: 200 µm; down: 100 µm. Data are represented as the mean ± SEM. * p-value < 0.05 between Wt mice and Pax8 +/- mice. + p-value < 0.05 between Wt mice and Pax8 -/- mice. & p-value < 0.05 between Wt mice and Wt T4 mice. # p-value < 0.05 between Wt mice and Pax8 +/- T4 mice. x p-value < 0.05 between Wt mice and Pax8 -/- T4.

Supplementary Table 1). Taken together these data suggest that severe loss of TH in Pax8-/- mice is lethal while modest reduction observed in Pax8 +/- mice is associated with altered metabolism as assessed by increased susceptibility to obesity and liver cancer.

We next assessed the impact of TH supplementation on health and longevity by treating or not, Wt, Pax8 +/- and Pax8 -/- male mice with T4. No differences were detected in circulating T4 levels in 21-day old T4-treated Wt (Wt T4) and T4-treated Pax8 +/- (Pax8 +/- T4) mice, which also exhibited normal liver histology (Figure 1A and 1I). At 8-month of age T4 levels were approximately 2-fold higher in Wt T4 and Pax8 +/- T4 mice as compared to Wt mice (Figure 1E). Although, energy intake was increased in both groups, Wt T4 and Pax8 +/- T4 mice remained significantly lighter than their untreated counterparts (Figure 1C and 1G). Lifespan was reduced in Wt T4 and Pax8 +/- T4 mice (Figure 1B). Lifespan was also shortened in T4-treated Pax8 -/- (Pax8 -/- T4) when compared to Wt mice (Figure 1B). Although T4 levels were similar to Wt mice in 21 days-old Pax8 -/- T4 mice, energy intake, body and organs weight was decreased in these mice (Figure 1A, 1D and Supplementary Figure 1D–1G). These data reveal that T4 supplementation in Wt and Pax8 deficient mice compromises lifespan.

The modulation of THs alters glucose homeostasis in adulthood

We recently reported that loss-of-function mutations in the human *PAX8* gene are associated with gestational diabetes mellitus and potentially with type 2 diabetes mellitus in males [33, 34]. As these mutations are also linked to hypothyroidism, we determined whether glucose metabolism was affected in adult (~7-month old) male Pax8 mice and whether T4 treatment could alleviate symptoms. Of note, Pax8 -/- and Pax8 -/- T4 mice were not included in these analyses due to their limited survival. Pax8 +/- mice exhibited mild glucose intolerance as compared to Wt mice even when values were corrected for basal glucose levels (Figure 2A–2B and Supplementary Figure 2A). Insulin levels during an oral glucose tolerance test (OGTT) were similar in Pax8 +/- mice, suggesting that glucose intolerance in these animals is not due to major defects in glucose-stimulated insulin secretion (Figure 2C–2D and Supplementary Figure 2B). We next performed an intraperitoneal (ip) pyruvate tolerance test (IPPTT) to investigate potential alterations in hepatic gluconeogenesis. Pax8 +/- mice exhibited increased glucose levels in blood compared to Wt mice at 60 and 120 minutes after the pyruvate load which led to an increase in the area under the curve (AUC) (Figure 2E–2F and Supplementary Figure 2C). Pax8 +/- mice displayed severe insulin resistance, as determined by increased AUC during the insulin tolerance test (ITT) (Figure 2G–2H and Supplementary Figure 2D). Confirming the insulin resistance observed in metabolic tests, western blots performed in liver extracts revealed a decrease in pSer473 Akt in Pax8 +/- mice (Figure 2I–2J). In contrast, pSer473 Akt levels were similar in gastrocnemius extracts of Pax8 +/- mice (Figure 2K–2L). Pax8 +/- mice exhibited an increased homeostatic assessment of insulin resistance (HOMA-IR) index, which was caused by fasting hyperinsulinemia (Figure 2M–2O). Pax8 +/- male mice also exhibited increased levels of glycated hemoglobin (HbA1c) (Figure 2P). Therefore, these results suggest that insulin resistance in Pax8 +/- mice is mainly due to impaired hepatic insulin sensitivity.

Wt T4 male mice exhibited restricted levels of circulating glucose during the ITT as well as in fasting conditions, as previously described in Wt T4-treated female mice (Figure 2G, H, M) [35]. Noticeably, the majority of metabolic tests indicated that T4 supplementation in Pax8 +/- mice normalized the metabolic phenotype of mild hypothyroid Pax8 +/- mice, suggesting that restricted TH levels in Pax8 +/- mice are responsible for the metabolic phenotype (Figure 2A–2H, 2M–2P).

High Fat Diet (HFD) feeding does not exacerbates the metabolic phenotype of Pax8 +/- mice

In order to investigate whether the phenotype observed in Pax8 +/- mice was further exacerbated by a metabolic challenge, we determined the effects of HFD feeding in adult Pax8 +/- mice. Metabolic parameters were assessed in ~7 month-old mice that had been on a HFD for up to 18 weeks in order to compare and contrast with experiments performed in standard diet-fed (STD) mice (Figures 1 and 2). Circulating T4 levels were slightly lower in HFD-fed Pax8 +/- mice when compared to HFD-fed Wt mice, while α-GSU levels remained similar (Figure 3A and Supplementary Figure 3A). Weight gain and energy intake were similar in HFD-fed Wt and HFD-fed Pax8 +/- mice (Figure 3B–3D). As expected, HFD-fed Wt mice exhibited compromised glucose clearance when compared to STD-fed Wt mice (Figures 2A–2B and 3E–3F). Glucose levels during an OGTT were similar between the different genotypes in HFD and comparable to STD-fed Pax8 +/- mice (Figure 2A–2B and 3E–3F). We observed a tendency towards decreased levels of circulating insulin at 15 minutes after a glucose load in HFD-fed Pax8 +/- mice (Figure 3G–3H). Glucose levels were lower in HFD-fed Pax8 +/- mice at all time-points during an IPPTT when compared to HFD-fed Wt mice, suggesting compromised pyruvate-induced hepatic gluconeogenesis (Figure 3I–3J). In contrast,

nonsignificant differences were observed between the different genotypes fed on HFD in an ITT, fasting blood glucose, fasting circulating insulin, HOMA-IR index, spatial learning and memory as well as in the weight of the main metabolic tissues at the time of sacrifice (Figure 3K–3O and Supplementary Figure 3B–3I). Overall these results indicate that Pax8 +/- mice suffer metabolic complications, irrespective of the energetic content of the diet.

Mild hypothyroid Pax8 +/- mice exhibit reduced basal metabolic rate and compromised physical performance

In order to further characterize the metabolic alterations associated with mild hypothyroidism in adult Pax8 +/- mice, we assessed several physiological parameters. Despite having increased body weight (Figure 1G), adult Pax8 +/- mice showed similar daily energy intake,

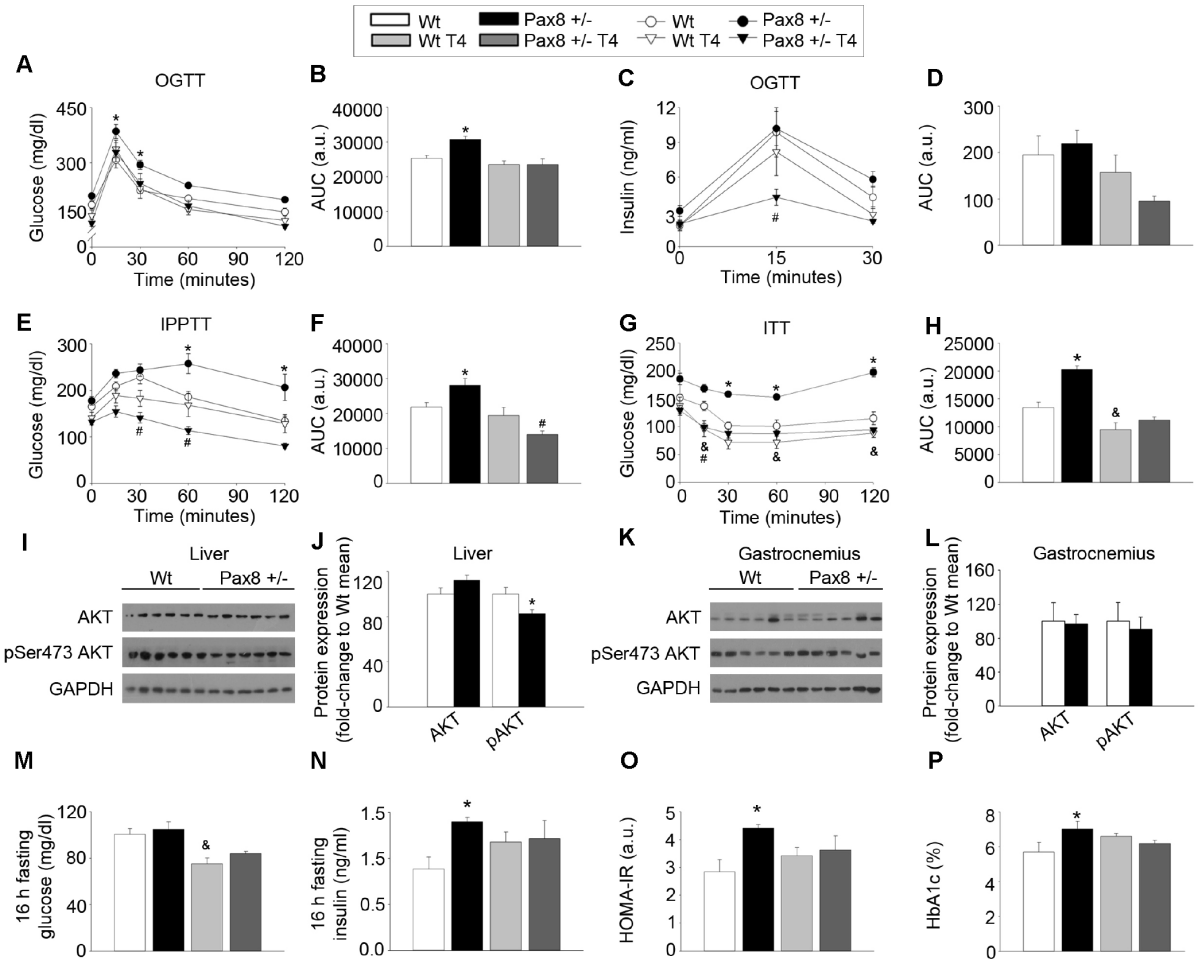

Figure 2. The modulation of THs alters glucose homeostasis in adulthood. (**A**) Circulating glucose levels during an OGTT. n = 8 per group. Repeated measurements two-way ANOVA. See also Supplementary Figure 2A. (**B**) AUC for the OGTT. Two-way ANOVA. (**C**) Circulating insulin levels during an OGTT. n = 8 per group. Repeated measurements two-way ANOVA. See also Supplementary Figure 2B. (**D**) AUC for the insulin levels in the OGTT. Two-way ANOVA. (**E**) Circulating glucose levels during an IPPTT. n = 8 per group. Repeated measurements two-way ANOVA. See also Supplementary Figure 2C. (**F**) AUC for the IPPTT. Two-way ANOVA. (**G**) Circulating glucose levels during an ITT. n = 8 per group. Repeated measurements two-way ANOVA. See also Supplementary Figure 2D. (**H**) AUC for the ITT. Two-way ANOVA. (**I**) Western blots showing total Akt and pSer473 Akt in liver extracts of Wt and Pax8 +/- mice. Mice were 9 month-old at time of death and were fasted 16 hours prior killing. (**J**) Densitometric analysis of western blots shown in panel I. n = 6 per group. T-test two tailed. (**K**) Western blots showing total Akt and pSer473 Akt in gastrocnemius extracts of Wt and Pax8 +/- mice. Mice were 9 month-old at time of death and were fasted 16 hours prior killing. (**L**) Densitometric analysis of western blots shown in panel K. n = 6 per group. T-test two tailed. (**M**) Glucose levels in blood after 16 hours of fasting. n = 8 per group. Two-way ANOVA. (**N**) Circulating insulin levels after 16 hours of fasting. n = 8 per group. Two-way ANOVA. (**O**) HOMA-IR. n= 8 per group. Two-way ANOVA. (**P**) Percentage of HbA1c. n = 7 per group. Two-way ANOVA. Data are represented as the mean ± SEM. Unless otherwise stated, mice were 7-month old at the time of experimentation. h: hours. a.u.: arbitrary units. * p-value < 0.05 between Wt mice and Pax8 +/- mice. & p-value < 0.05 between Wt mice and Wt T4 mice. # p-value < 0.05 between Wt mice and Pax8 +/- T4 mice.

water intake and reduced fasting-induced energy intake when compared to Wt mice (Figure 4A–4B and Supplementary Figure 4A–4B). No differences were observed in either fecal lipid content or body temperature (Figure 4C–4D). *In vivo* indirect calorimetry indicated that the respiratory exchange ratio (RER) was unaffected (Figure 4E). In contrast, heat production was decreased in Pax8 +/- mice specifically during light-time, a time at which mice are less active (Figure 4F–4H). During dark-time Pax8 +/- mice exhibited a greater spontaneous locomotor activity and ran longer distances when compared to their Wt counterparts (Figure 4G–4H). Heat production was similar between different genotypes at that specific part of the day cycle (Figure 4F). The analysis of circulating lipids indicated that total cholesterol levels were lower in Pax8 +/- mice as a result of reduced HDL with no changes in triglyceride levels (Figure 4I–4J). Lower levels of HDL may stem from liver dysfunction/damage. Nonetheless, blood levels of glutamic-pyruvic transaminase (Gpt) and glutamic oxaloacetic transaminase (Got) were lower and unaltered, respectively, in Pax8 +/- mice as compared to Wt mice

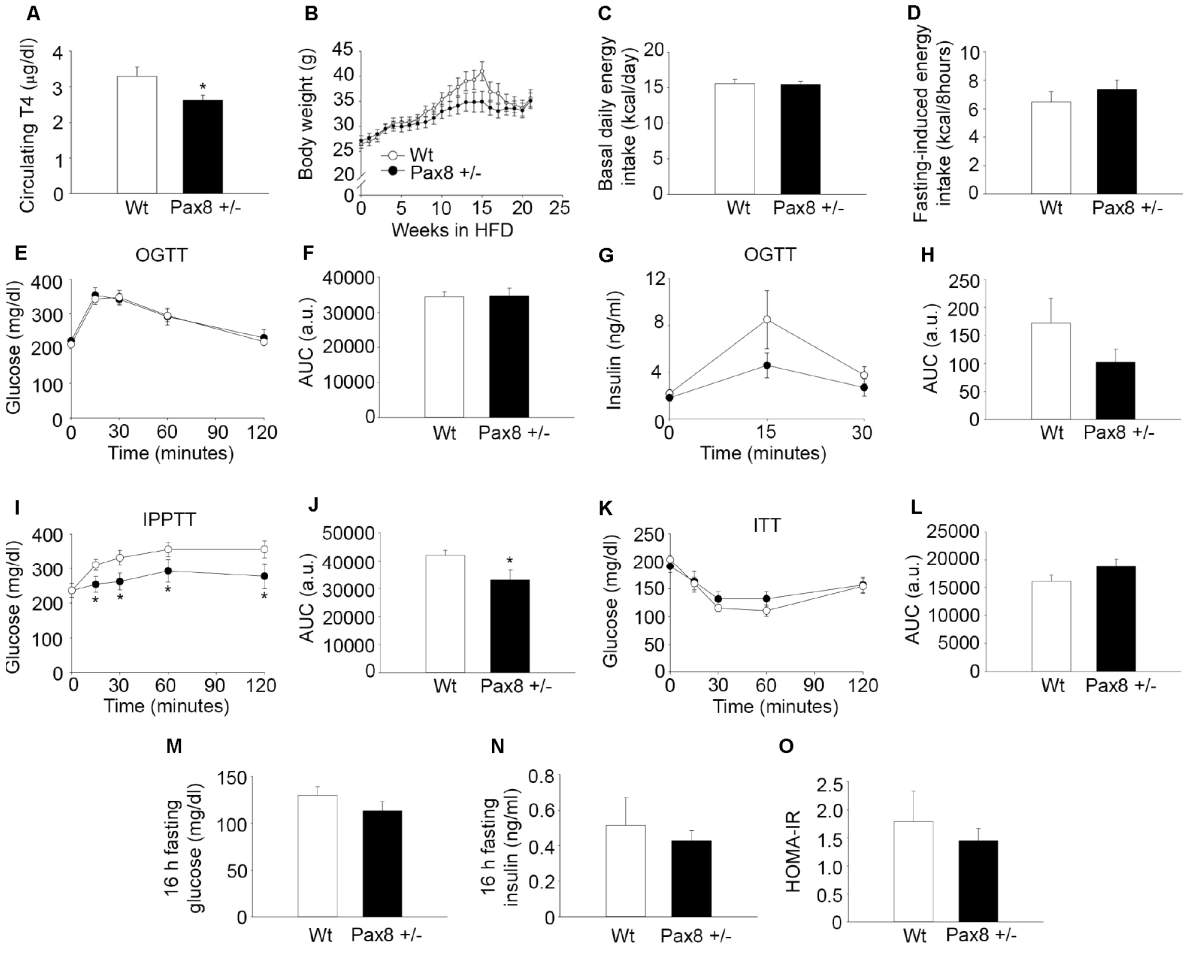

Figure 3. High fat diet (HFD) feeding does not exacerbates the metabolic phenotype of Pax8 +/- mice. (**A**) T4 levels in serum (18 weeks of HFD feeding). n = 8 Wt, n = 9 Pax8 +/-. T-test two tailed. (**B**) Body weights during HFD feeding. n = 15 Wt, n = 14 Pax8 +/-. Repeated measurements two-way ANOVA. (**C**) Basal daily energy intake at 6 months of life (13 weeks of HFD feeding). n = 8 Wt, n = 9 Pax8 +/-. T-test two tailed. (**D**) Fasting induced energy intake (17 weeks of HFD feeding). n = 8 Wt, n = 9 Pax8 +/-. T-test two tailed. (**E**) Circulating glucose levels during an OGTT at 6 months of life (14 weeks of HFD feeding). n = 13 Wt, n = 11 Pax8 +/-. Repeated measurements two-way ANOVA. (**F**) AUC for glucose levels during the OGTT. T-test two tailed. (**G**) Insulin levels in plasma during an OGTT (17 weeks of HFD feeding). n = 8 per group. Repeated measurements two-way ANOVA. (**H**) AUC for insulin levels during the OGTT. T-test two tailed. (**I**) Circulating glucose levels during the IPPTT (15 weeks of HFD feeding). n = 13 Wt, n = 10 Pax8 +/-. Repeated measurements two-way ANOVA. (**J**) AUC for the IPPTT. T-test two tailed. (**K**) Glucose levels in blood during the ITT (16 weeks of HFD feeding). n = 9 per group. Repeated measurements two-way ANOVA. (**L**) AUC for the ITT. T-test two tailed. (**M**) Glucose levels in blood after 16 hours of fasting (18 weeks of HFD feeding). n = 8 per group. T-test two tailed. (**N**) Circulating insulin after 16 hours of fasting (18 weeks of HFD feeding). n = 8 per group. T-test two tailed. (**O**) HOMA-IR (18 weeks of HFD feeding). n = 8 per group. T-test two tailed. Data are represented as the mean ± SEM. * p-value <0.05. Unless otherwise stated, mice, were 7-month old at the time of experimentation.

indicating normal liver function (Figure 4K–4L). Mild hypothyroid Pax8 +/- mice performed poorly on rotarod and wire hang physical tests (Figure 4M–4N). Histological analyses of gastrocnemius by optic microscopy and electron microscopy indicated similar proportion of type I and type II myofibers, as well as comparable morphology and ultrastructure of subsarcolemmal and intermyofibrillar mitochondrial populations, suggesting that compromised physical activity is likely caused by the increased body weight rather than detrimental functional effects in skeletal muscle (Supplementary Figure 4C–4F). Finally, Pax8 +/- and Wt mice shared identical spatial learning and memory, indicating no alterations in neurocognitive function (Supplementary Figure 4G–4L). These results indicate that Pax8 +/- mild hypothyroid male mice exhibit an overall unhealthy status which involves a lower basal metabolic rate, a clinical feature associated with human hypothyroidism [36].

Mild hypothyroid Pax8 +/- mice accumulate ectopic lipid depositions

Histological analysis of the four predominant organs involved in metabolic homeostasis revealed larger adipocytes and aberrant lipid accumulation in the liver and gastrocnemius of 9-month old Pax8 +/- mice (Figure 5A). Although pancreatic islet architecture

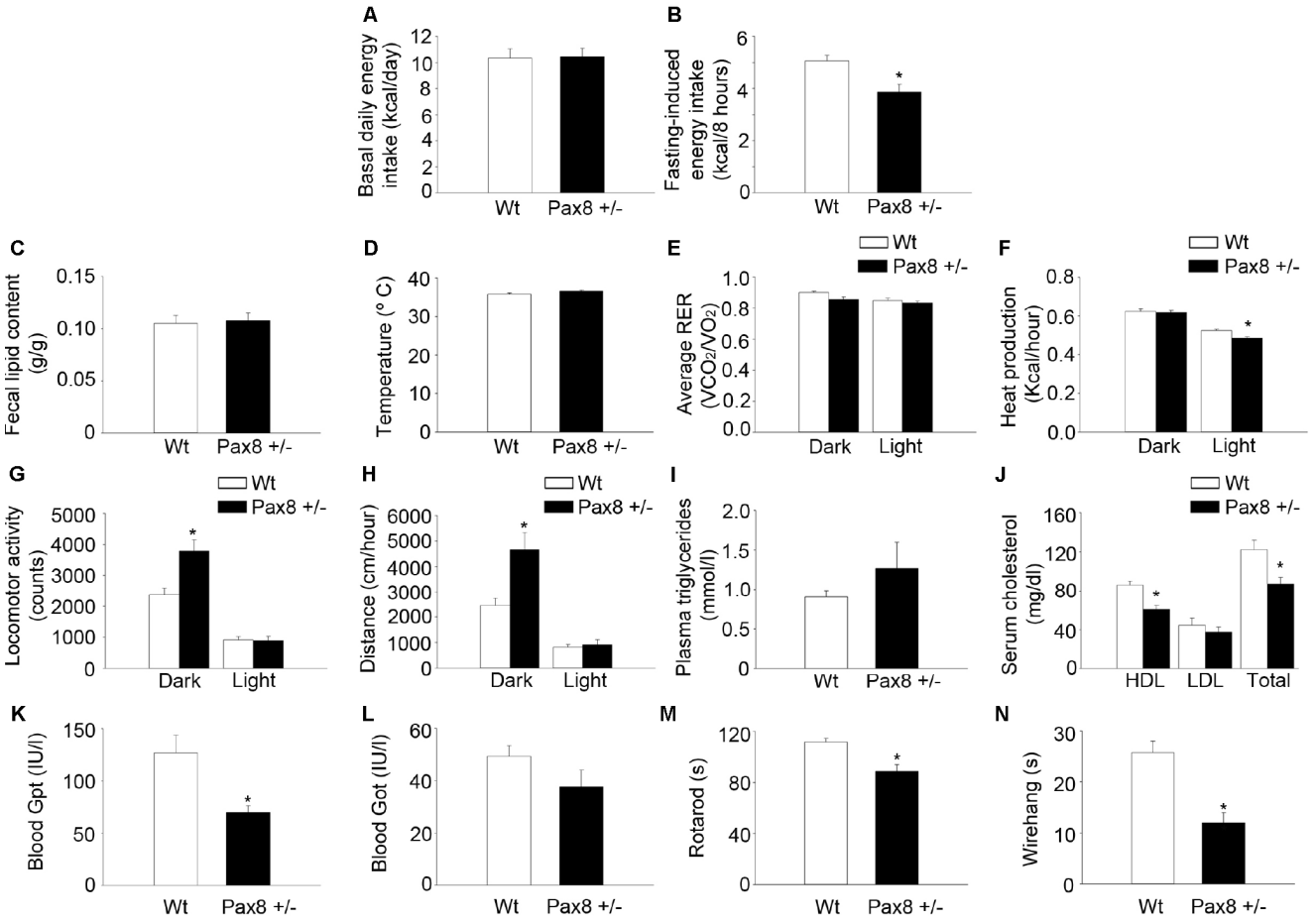

Figure 4. Mild hypothyroid Pax8 +/- mice exhibit reduced basal metabolic rate and compromised physical performance. (**A**) Basal daily energy intake per day at 10-12 months of life. n = 5 Wt, n = 4 Pax8 +/- (the n reflects the number of cages). (**B**) Fasting-induced energy intake at 10-12 months of life. n = 21 Wt, n = 14 Pax8 +/-. (**C**) Lipid content in faeces. n = 7 Wt, n = 6 Pax8 +/-. (**D**) Body temperature. n = 12 Wt, n = 8 Pax8 +/-. (**E**) Determination of RER in metabolic cages. n = 8 Wt, n = 7 Pax8 +/-. (**F**) Determination of heat production in metabolic cages. n = 8 Wt, n = 7 Pax8 +/-. (**G**) Determination of spontaneous locomotor activity (y + x axis) in metabolic cages. n = 8 Wt, n = 7 Pax8 +/-. (**F**) Determination of run distance in metabolic cages. n = 8 Wt, n = 7 Pax8 +/-. (**H**) Triglyceride concentration in plasma. n = 18 Wt, n = 13 Pax8 +/-. (**I**) Total cholesterol, HDL and LDL/VLDL levels in serum. n = 7 per group. (**J**) Blood levels of Gpt. n = 7 per group. (**K**) Blood levels of Got. n = 7 per group. (**L**) Time to fall from an accelerating rotarod at 7-10 months of life. n = 27 Wt, n = 20 Pax8 +/-. (**M**) Time to fall in wire hang test at 7-10 months of life. n = 27 Wt, n = 20 Pax8 +/-. Data are represented as the mean ± SEM. Unless otherwise stated, mice were 7-month old at the time of experimentation. * p-value < 0.05. T-test two tailed.

appeared normal without evidence of lipid accumulation and insulin levels were not altered in adult Pax8 +/- mice during an OGTT (Figure 2C–2D and Figure 5A), at 9-month old Pax8 +/- mice exhibited a reduced percentage of insulin-expressing pancreatic β cells and a concomitant increase in somatostatin-expressing pancreatic δ-cells (Figure 5B–5E). These differences were not observed at weaning (21 days-old mice) (Supplementary Figure 5A–5D). To better understand the impact of mild hypothyroidism on pancreatic islets, we performed a genome-wide transcriptomic analysis. The expression of 232 genes was upregulated (fold-change ≥ 2.5; p value ≤ 0.05) while the expression of 119 genes was downregulated in islets of Pax8 +/- mice (fold-change ≤-2.5; p value ≤ 0.05). Among the most up-regulated genes were secretagogin (*scgn*), the proprotein convertase Subtilisin/Kexin Type 1 Inhibitor (*Pcsk1n*) and the solute carrier family 2 member 5, also known as glucose transporter 5 (*Slc2a5*/*Glut5*), which encode for proteins involved in β-cell turnover, glucose uptake (preferentially in α-cells) and insulin processing and secretion (Figure 5F and Supplementary Table 2) [37, 38]. Top significantly downregulated genes included genes encoding for the glucose transporter 1 (*Slc2a1*/*Glut1*), and the Heme-oxigenase1 (*Hmox1*), which encode for glucose transporters and antioxidant proteins, respectively (Figure 5F and Supplementary Table 2). Analyses using the Ingenuity Pathway Analysis and Transcriptome Analysis Console platforms for genome-wide expression analyses indicated that oxidative phosphorylation (up-regulated) and antioxidant stress response (down-regulated) were among the most modulated pathways in pancreatic islets isolated from mild hypothyroid Pax8 +/- mice (Figure 5G and Supplementary Figure 5E–5G).

Consistent with lipid accumulation, tissue weight at sacrifice (9-month old) indicated that the white adipose tissue (WAT) of Pax8 +/- mice was heavier, even when corrected by total body weight, and was composed of larger adipocytes when compared to the WAT of Wt mice (Figure 5A, 5H–5J). Furthermore, liver and gastrocnemius of Pax8 +/- mice accumulated greater amounts of triglycerides (Figure 5K–5L). Given that THs are potent modulators of fatty acid composition and storage, and that aberrant accumulation of certain lipid species lead to cell dysfunction and death (lipotoxicity), we performed lipidomic analysis on WAT, liver and gastrocnemius [39]. The analysis of WAT indicated that mild hypothyroid Pax8 +/- mice accumulated a higher percentage of oleic acid (18:1n9) as well as increased proportion of triglycerides formed by 3 oleic acids (OOO), with a concomitant reduction of the proportion of triglycerides formed by other fatty acids such as palmitic acid and linolenic acid (PLL) (Figure 5M–5N). However, the percentage of different polar lipid species was comparable to Wt mice, suggesting the absence of major alterations in cellular membrane integrity or fluidity (Supplementary Figure 5H). Similarly, the percentage of 18:1n9, as well as 18:1n7, fatty acid species was higher in the liver of Pax8 +/- mice as compared to Wt mice, while no significant differences were observed in the gastrocnemius (Figure 5M). The analysis of triglyceride species in liver lysates indicated a reduction of certain triglycerides composed by more than one poli-unsaturated fatty acid and a concomitant increase in triglycerides composed by saturated fatty acids, such as stearic acid (Figure 5N). No differences in proportions of polar lipid species were found in liver and gastrocnemius tissues (Supplementary Figure 5H). RNA and protein isolations of liver tissue exhibited a marked modulation on genes and proteins involved in lipid transport, synthesis and catabolism (Figure 5O–5Q). Transcript levels of *Srebp-1c*, *Srebp2* which are involved in fatty acid and cholesterol biosynthesis, respectively, were induced in the liver but not in the gastrocnemii (*Srebp-1c*) of Pax8 +/- mice (Figure 5O and Supplementary Figure 5I). Although the liver of Pax8 +/- mice exhibited more lipid droplets, the expression level of fatty acid synthase (Fas) was restricted, suggesting that free fatty acid supplies for liver triglyceride synthesis are likely provided by circulating lipoproteins (Figure 5P–5Q). Consistent with this premise, expression of the fatty acid scavenger receptor *Cd36* was significantly increased in liver of Pax8 +/- mice (Figure 5O). In parallel, RNA expression levels of the medium chain acyl-CoA dehydrogenase (*Mcad*) and protein expression levels of acetyl-coenzyme A acyltransferase 2 (Acaa2), which catalyze essential steps on the mitochondrial β-oxidation of fatty acids, were markedly increased in the livers of Pax8 +/- mice compared to Wt, suggesting greater hepatic beta oxidation (Figure 5O–5Q). No significant differences were observed in mRNA and/or protein levels of pro-inflammatory markers (Figure 5O–5Q). None of the above alterations were apparent in the gastrocnemius (Supplementary Figure 5I–5K). These results indicate that mild hypothyroidism in Pax8 +/- mice does not result in an inflammatory milieu, which is commonly found in individuals suffering metabolic disorders [40].

Mild hypothyroidism produces mitochondrial dysfunction and accumulation of oxidative damage in Pax8 +/- mice

Mitochondrial dysfunction and oxidative stress have been detected in patients with non-alcoholic fatty liver disease (NAFLD) [41, 42]. Therefore, we next investigated whether mitochondria content and function were altered in Pax8 +/- mice. Although transcript and protein levels of Pgc1-α, a master regulator of

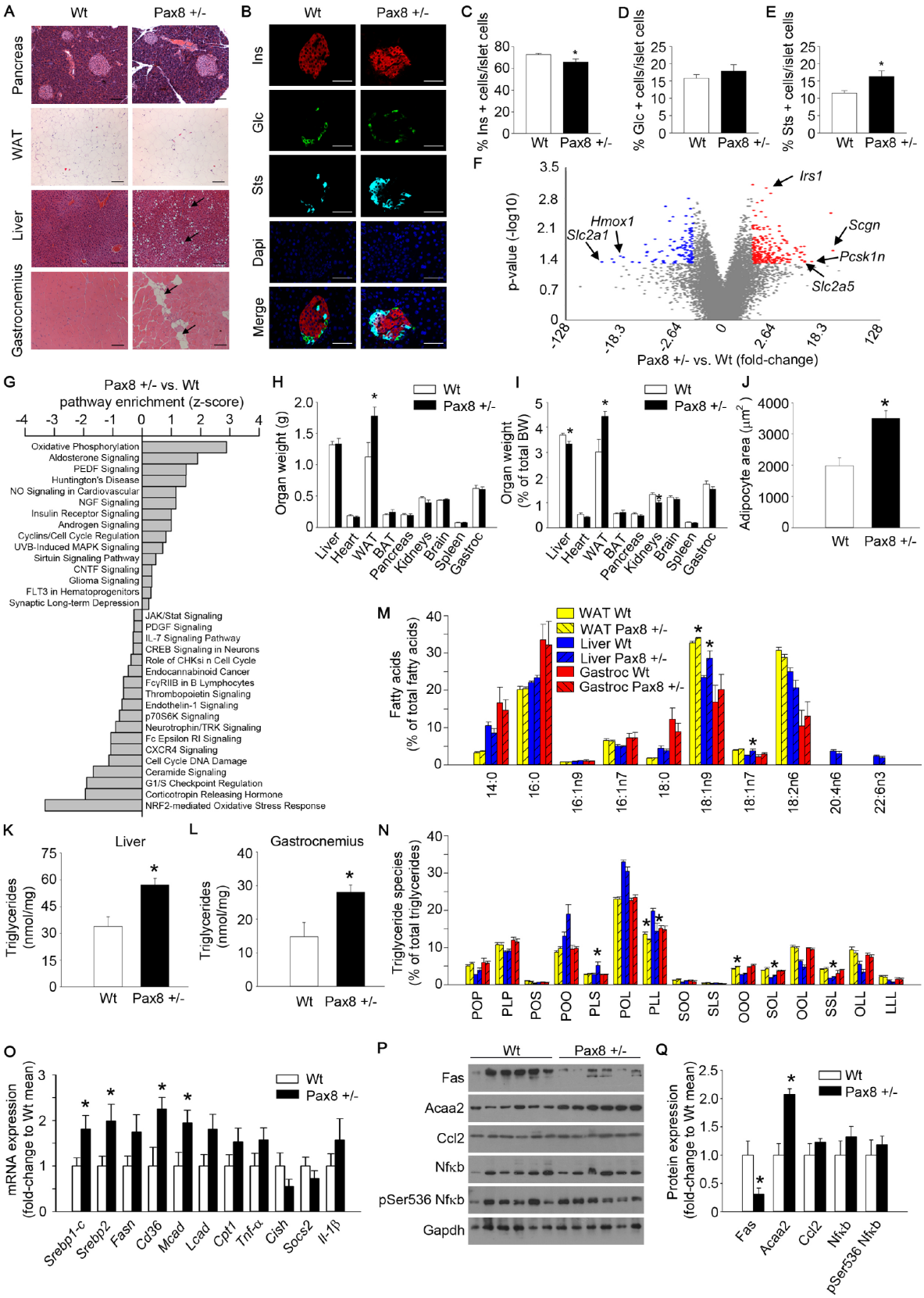

Figure 5. Mild hypothyroid Pax8 +/- mice accumulate ectopic lipid depositions. (**A**) Representative images of hematoxylin and eosin staining of WAT, gastrocnemius, pancreas and liver of Wt and Pax8 +/- mice. Arrows indicate adipocyte infiltrations in gastrocnemius and lipid droplets in liver tissue. WAT: n = 6 Wt, n = 4 Pax8 +/-; gastrocnemius: n = 6 per group; pancreas: n = 3 per

group; liver: n = 6 per group; Scale bar = 100 µm. (**B**) Representative immunofluorescence images of pancreatic sections from untreated Wt and Pax8 +/- male mice at 9 months of age. Scale bar: 50 µm. Ins: insulin. Glc: glucagon. Sts: somatostatin. n = 5 Wt, n = 4 Pax8 +/-. (**C**) Percentage of insulin positive cells in islet cells at 9 months of age. n = 5 Wt, n = 4 Pax8 +/-. T-test two tailed. (**D**) Percentage of glucagon positive cells in islet cells at 9 months of age. n = 5 Wt, n = 4 Pax8 +/-. T-test two tailed. (**E**) Percentage of somatostatin positive cells in islet cells at 9 months of age. n = 5 Wt, n = 4 Pax8 +/-. T-test two tailed. (**F**) Volcano plot showing the fold change and statistical significance of genes expressed in pancreatic islets. Statistical analysis was performed using Transcription Analysis Console using default parameters. Arrows indicate specific dots of highlighted genes. See also Supplementary Figure 5E–5G. n = 3 per group. (**G**) Analysis of significantly modulated annotated canonical pathways in pancreatic islets using Ingenuity Pathway Analysis platform. Statistical analysis was performed using Ingenuity Pathway Analysis using significantly modulated genes. n = 3 per group. (**H**) Tissues weight. n = 6 per group. T-test two tailed. (**I**) Tissues weight corrected by total body weight. n = 6 per group. T-test two tailed. (**J**) Quantification of adipocyte area. n = 6 Wt, n = 4 Pax8 +/-. T-test two tailed. (**K**) Triglyceride content per mg of protein in liver. n = 6 Wt, n = 4 Pax8 +/-. T-test two tailed. (**L**) Triglyceride content per mg of protein in gastrocnemius. n = 5 Wt, n = 4 Pax8 +/-. T-test two tailed. (**M**) Lipidomic analysis depicting percentages of the different species of fatty acids in WAT, liver and gastrocnemius. n = 5 Wt, n = 6 Pax8 +/-. Two-way ANOVA. See also Supplementary Figure 5H. (**N**) Lipidomic analysis depicting percentages of triglyceride species in WAT, liver and gastrocnemius. P: Palmitic acid. O: Oleic acid. L: Linoleic acid. S: Stearic acid. n = 5 Wt, n = 6 Pax8 +/-. Two-way ANOVA. (**O**) mRNA expression of genes involved in lipid synthesis/import and inflammation in livers from Wt and Pax8 +/- mice. *Srebp1-c*: n = 6 per group. *Srebp2*: n = 6 per group. *Fasn*: n = 5 Wt, n = 6 Pax8 +/-. *Cd36*: n = 6 Wt, n = 5 Pax8 +/-. *Mcad*: n = 6 per group. *Lcad*: n = 6 per group. *Cpt1*: n = 6 per group. *Tnf-α*: n = 5 Wt, n = 6 Pax8 +/-. *Cish*: n = 4 Wt, n = 5 Pax8 +/-. *Socs2*: n = 4 Wt, n = 4 Pax8 +/-. *Il-1β*: n = 6 per group. T-test two tailed. (**P**) Western blots showing protein expression levels of markers of lipid metabolism and inflammation in liver lysates. n = 6 per group. (**Q**) Densitometric analysis of western blots shown in panel P. n = 6 per group. T-test two tailed. Data are represented as the mean ± SEM. Mice were 9 month-old at the time of killing. vs: versus. * p-value < 0.05.

mitochondrial biogenesis, were increased in the liver of Pax8 +/- mice, the expression of several mitochondrial proteins was similar in mild hypothyroid Pax8 +/- mice (Figure 6A–6C). In agreement with similar mitochondrial content, the liver of Pax8 +/- mice displayed similar mitochondrial DNA to nuclear DNA ratio and citrate synthase activity (Figure 6D–6E). Likewise, no differences were detected between genotypes in the specific enzymatic activities of complexes I+III (NADH-cytochrome *c* oxidoreductase activity) and II+III (succinate-cytochrome *c* oxidoreductase activity) in liver lysates, even when corrected to citrate synthase activity (Figure 6F–6I). Interestingly, gene expression levels of *Atp5a1*, a subunit of complex V involved in ATP synthesis, was increased in the liver of Pax8 +/- mice (Figure 6A). We also observed a marked reduction in Ucp2 expression in the liver of Pax8 +/- mice, consistent with this uncoupling protein being a direct target of THs (Figure 6A–6C). Protein levels of pThr172 Ampk were reduced in liver of Pax8 +/- mice compared to Wt, indicative of a rich energetic status in hepatic tissue (Figure 6B–6C). Remarkably, superoxide generation in mitochondrial complexes was significantly increased in the liver of Pax8 +/- animals, even when corrected to citrate synthase activity (Figure 6J–6K). To assess net effects in mitochondrial performance, we determined *in vivo* oxygen consumption in primary hepatocytes isolated from Wt and Pax8 +/- mice. Although the extracellular acidification rate (ECAR) under basal conditions was similar in both experimental groups, oxygen consumption was reduced in Pax8 +/- hepatocytes (Figure 6L–6M). Interestingly, carbonyl cyanide 4-(trifluoromethoxy) phenylhydrazone (FCCP)-induced maximal oxygen consumption was minimal in the hepatocytes of Pax8 +/- mice (Figure 6L). Confirmatory experiments using the 3-(4,5-dimethylthiazol-2-yl)-2,5-diphenyltetrazolium bromide (MTT) test indicated that metabolic activity was reduced in primary hepatocytes isolated from in Pax8 +/- mice (Figure 6N). We next determined the protein levels and enzymatic activities of several antioxidant proteins (Figure 6O–6Q). Results indicated that liver extracts from Pax8 +/- mice exhibited increased cytosolic superoxide dismutase (Sod cyt) and reduced glutathione S transferase (Gst) protein levels and enzymatic activities, suggesting that hepatic tissue of Pax8 +/- mice senses a pro-oxidant status and modulate the expression/activity of certain antioxidant proteins (Figure 6P–6Q). In addition, protein levels of growth arrest DNA damage 153 (Gadd 153) were increased and Lc3b-I and Lc3b-II levels were reduced in liver extracts of Pax8 +/- mice, indicating that hepatic cells are under cellular stress and that autophagy induction may be impaired in the liver of Pax8 +/- mice (Figure 6P–6Q). Consistent with increased ROS generation and altered antioxidant activity, determinations of lysine-4-hydroxinonenal (Lys-4-HNE) levels, which result from lipid peroxidation, revealed a significant increase in the liver of Pax8 +/- mice (Figure 6R–6S). Despite a dramatic increase in Pgc1-α protein expression, no differences were detected in RNA and protein expression levels of mitochondrial genes/proteins including Ucp2 or in respiratory complex activities in gastrocnemius extracts of Pax8 +/- mice (Supplementary Figure 6A–6I). Although mitochondrial ROS generation and antioxidant protein levels were similar in both Pax8 +/- and Wt mice, Lys-4-HNE levels were higher in Pax8 +/-

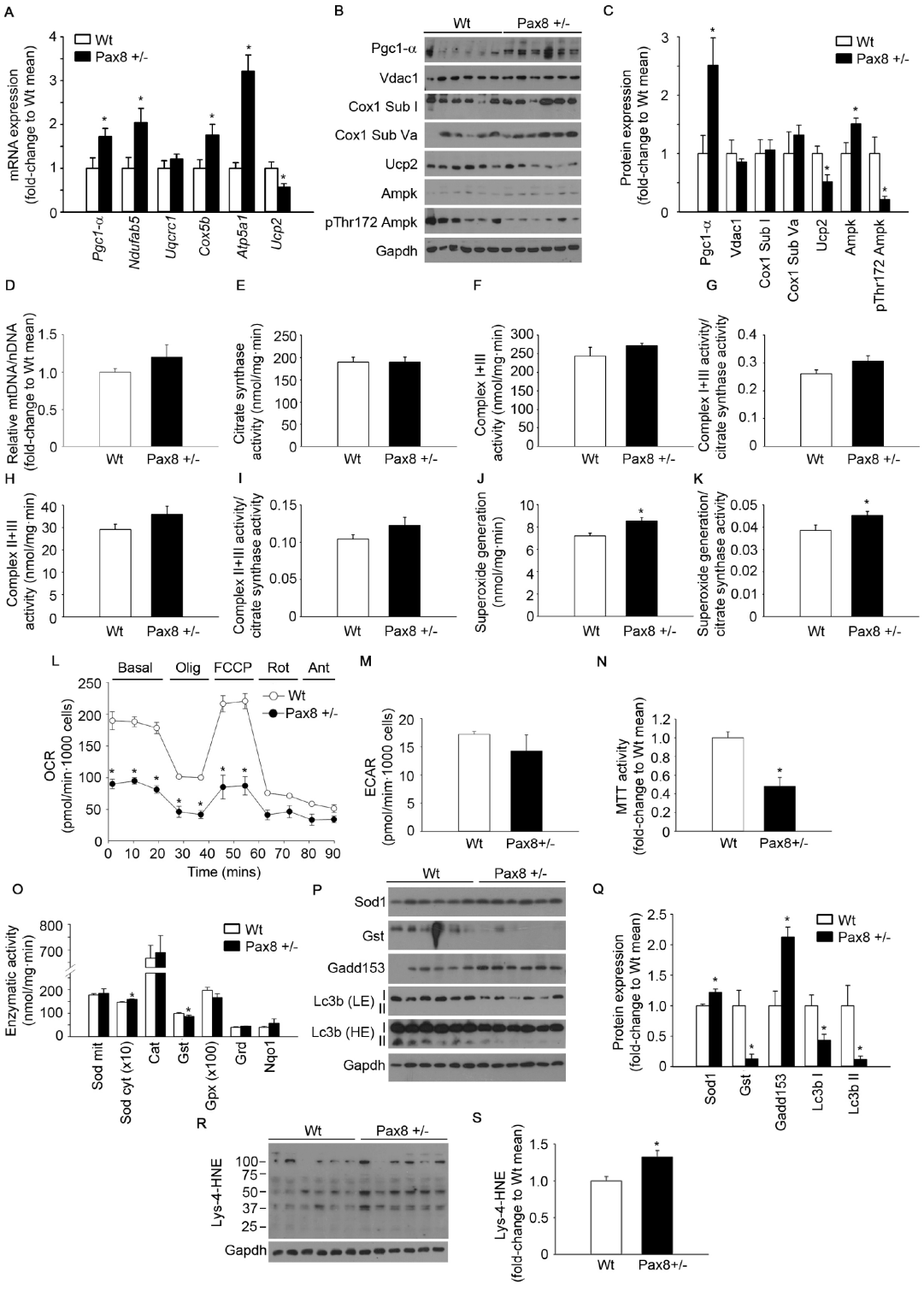

Figure 6. Mild hypothyroidism produces mitochondrial dysfunction and accumulation of oxidative damage in Pax8 +/- mice. (**A**) mRNA expression of genes involved in mitochondrial biogenesis and mitochondrial function in liver. *Pgc1-α*: n = 6 per group. *Ndufab5* = n = 6 per group. *Uqcrc1*: n = 6 per group. *Cox5b*: n = 6 per group. *Atp5a1*: n = 5 Wt, n = 6 Pax8 +/-. *Ucp2*: n = 5 per group. (**B**) Western blots showing expression levels of proteins involved in mitochondrial biogenesis/function as well as Ampk and its phosphorylated isoform in liver lysates. n = 6 per group. (**C**) Densitometric analysis of western blots shown in panel B. n = 6 per group. (**D**) Relative mitochondrial DNA content in liver isolations. n = 6 per group. (**E**) Citrate synthase activity in liver extracts. n = 6 per group. (**F**) Complex I+III activity in liver extracts. n = 6 per group. (**G**) Complex I+III activity corrected by citrate synthase activity in liver extracts. n = 6 per group. (**H**) Complex II+III activity in liver extracts. n = 6 per group. (**I**) Complex II+III activity corrected by citrate synthase activity in liver extracts. n = 6 per group. (**J**)

Superoxide generation in mitochondrial complexes in liver extracts. n = 6 per group. (**K**) Superoxide generation in mitochondrial complexes corrected by citrate synthase activity in liver extracts. n = 6 per group. (**L**) Oxygen consumption rate in primary hepatocytes. n = 3 per group. (**M**) Extracellular acidification rate in primary hepatocytes. n = 3 per group. (**N**) MTT test to determine the metabolic activity (NADH-oxidase) of primary hepatocytes. n = 4 per group. (**O**) Antioxidant enzymatic activities in liver lysates. Sod mit: n = 6 per group. Sod cyt: n = 5 per group. Cat: n = 5 Wt, n = 6 Pax8 +/-. Gst: n = 5 per group. Gpx: n = 5 per group. Grd: n = 6 Wt, n = 5 Pax8 +/-. Nqo1: n = 5 Wt, n = 6 Pax8 +/-. Sod mit: Sod mitochondrial. Sod cyt: Sod cytosolic. (**P**) Western blots showing expression levels of antioxidant, stress response and autophagy induction proteins in liver lysates. LE = Low exposure. HE = High exposure. n = 6 per group. (**Q**) Densitometric analysis of western blots shown in panel **P**. (**R**) Western blot showing Lys-4-HNE staining in liver extracts. n = 6 per group. (**S**) Densitometric analysis of the western blot shown in panel **R**. Mice were 9 month-old at the time of killing. Data are represented as the mean ± SEM. * p-value < 0.05. T-test two tailed.

mice (Supplementary Figure 6J–6O). Taken together, these indicate that, in liver tissue, the antioxidant system is unable to scavenge increased ROS production, leading to the accumulation of oxidative damage in a process that is known to be involved in carcinogenesis.

DISCUSSION

Harnessing mechanisms governing organismic senescence is central to aging biology in order to develop approaches for healthy aging, a priority of current times. Herein, we tackle this problematic by resolving the controversy on whether the modulation of TH levels is beneficial or detrimental for the health and welfare of individuals. Although our study only included male mice, representing a limitation of our work, we provide evidence that either the lack or chronic supplementation of TH reduces life expectancy while mild hypothyroidism compromises healthspan without extending lifespan. Our study also substantiates that patients bearing *PAX8* mutations resulting in mild hypothyroidism, are prone to develop diabetes (type 2 and gestational), as evidenced by our previous study [33], and likely to develop liver cancer. With regard to the latter, both, hypothyroidism and SNP variants in the *PAX8* gene, have been associated with the development of hepatocellular carcinomas in Asian and Non-Hispanic white cohorts [43, 44].

Mice that lack the ability to produce TH exhibited very low body weight and limited survival, dying around weaning (Figure 7). This fact is particularly interesting since the longest-living laboratory mice are characterized by low to barely detectable levels of THs. Our findings indicate that the modulation of other hormones (*e.g.* growth hormones) must be exclusively responsible for the increases in lifespan in other dwarf mice such as the Snell, Ames and Laron mice [5, 7, 9–11]. Our data reveal that T4 supplementation in Pax8 ablated mice extended life expectancy when compared to untreated Pax8 -/- mice while the same treatment reduced by half lifespan in both Wt and Pax8 heterozygous animals. Combined with our previous work [35], our results support that TH supplementation leading to hyperthyroidism produces an improvement on markers of metabolic health, such as reduced age-dependent body weight gain and fasting glycaemia but that chronic treatment results in toxicity and reduced lifespan. These results are consistent with human studies demonstrating that life expectancy for both, men and women, decreased with higher levels of TH [45], and highlights the strict requirement to maintain TH levels within physiological levels during replacement therapy to maintain the health and welfare of patients (Figure 7) [46].

Pax8 heterozygous mice that displayed mild reduction in TH levels did not live longer compared to wild type mice and featured mild obesity, insulin resistance, increased WAT weight, triglyceride accumulation in skeletal muscle, liver steatosis as well as preponderance to develop liver cancer with age. These metabolic alterations recapitulate alterations observed in patients suffering hypothyroidism such as, metabolic syndrome and NAFLD, Type 2 diabetes and hepatocellular carcinomas [28, 33, 43, 44, 47–49]. Therefore, we propose the Pax8 +/- mouse as a valuable experimental model to further dissect the cellular and molecular mechanisms associated with mild hypothyroidism and hypothyroidism-related pathologies. However, Pax8 +/- mice did not exhibit a pro-inflammatory milieu in the liver or the skeletal muscle, which is commonly associated with metabolic disorders [40]. Similar to humans, TH supplementation reversed diseases hallmarks in Pax8 +/- mice, supporting the premise that reduced TH levels rather than *Pax8* haploinsufficiency or direct transcriptional effects of Pax8 targets convey these pathophysiological conditions [47]. Further substantiating this premise is the lack of *Pax8* expression in liver, WAT and skeletal muscle. The phenotype of Pax8 heterozygous mice did not worsen when fed a HFD, indicating that mice are metabolically stressed independent of diet.

Although pancreatic islets appeared architecturally normal at weaning, a reduction in the percentage of beta cell with a concomitant increase in delta cells was observed in adult mice. Whether the modulation of endocrine populations in pancreatic islets in adulthood is compensatory mechanism or whether these are independent cellular events remains to be clarified. Nonetheless, TH facilitate maturation of human fetal islet beta cells as well as neonatal rat beta

cells, a process mediated by up-regulation of the beta cell-enriched transcription factor MafA [50, 51]. We also previously demonstrated that TH delayed beta cell loss under stress conditions and that mutations on *PAX8* are found in patients developing gestational diabetes [33, 35]. It is therefore tempting to speculate that hypothyroidism in Pax8 +/- mice hinders postnatal beta cell maturation with subsequent increased in the susceptibility to stress-induced apoptosis with age, favouring the replacement of beta cells by delta cells that do not require MafA. Evidence for stress-induced apoptosis is provided by the transcriptome profile of Pax8 +/- islets that reveal, on one hand, higher metabolism-secretion coupling, likely due to hypothyroidism-induced insulin resistance, and, on the other hand, lower antioxidant defenses, likely resulting in β-cell exhaustion and apoptosis at long-term. Further studies are required to assess the impact of hypothyroidism on delta cell fate.

Liver lipidomic profiling revealed oleic acid was enriched in Pax8 +/- mice consistent with a previous study demonstrating that increased intake of this fatty acid promotes hepatoma progression by reducing the expression of Pten [52]. In contrast, other studies have reported that oleic acid is beneficial rather than detrimental due to its capacity to revert palmitic acid-induced hepatic insulin resistance and apoptosis and that the dietary palmitic acid:oleic acid ratio impacts diabetes risk in human [53]. Contextually, hypothyroidism may short-circuit the beneficial role of oleic acid by skewing accumulation of oleic acid and triglycerides, independent of palmitic acid, which long-term may cause NAFLD. Consistent with this premise and in line with results observed in Pax8 +/- mice, oleic acid was markedly increased whereas total serum cholesterol was decreased in mice over-expressing SREBPs, which are downstream targets of the TH signalling pathway [54]. Engorgement of hepatic tissue with lipids was likely the cause of insulin resistance, as evidenced by decreased Akt phosphorylation and contributed to the energy-rich status, as revealed by decreased AMPK phosphorylation. Consistent with this status several markers of mitochondrial beta oxidation were enhanced. Nonetheless, we observed mitochondrial dysfunction as revealed by reduced oxygen consumption in primary live hepatocytes and increased mitochondrial superoxide generation in liver lysates. Of interest, *Cd36* expression, a long-chain fatty acid scavenger receptor found to be increased in the liver of Pax8 +/- mice, is also highly expressed in patients with NAFLD and appears to be required for fatty acid-induced ROS production [55, 56]. In parallel the expression and enzymatic activity of several antioxidant response proteins was altered with a net accumulation of oxidative damage. These data suggest that hepatic tissue senses a pro-oxidant

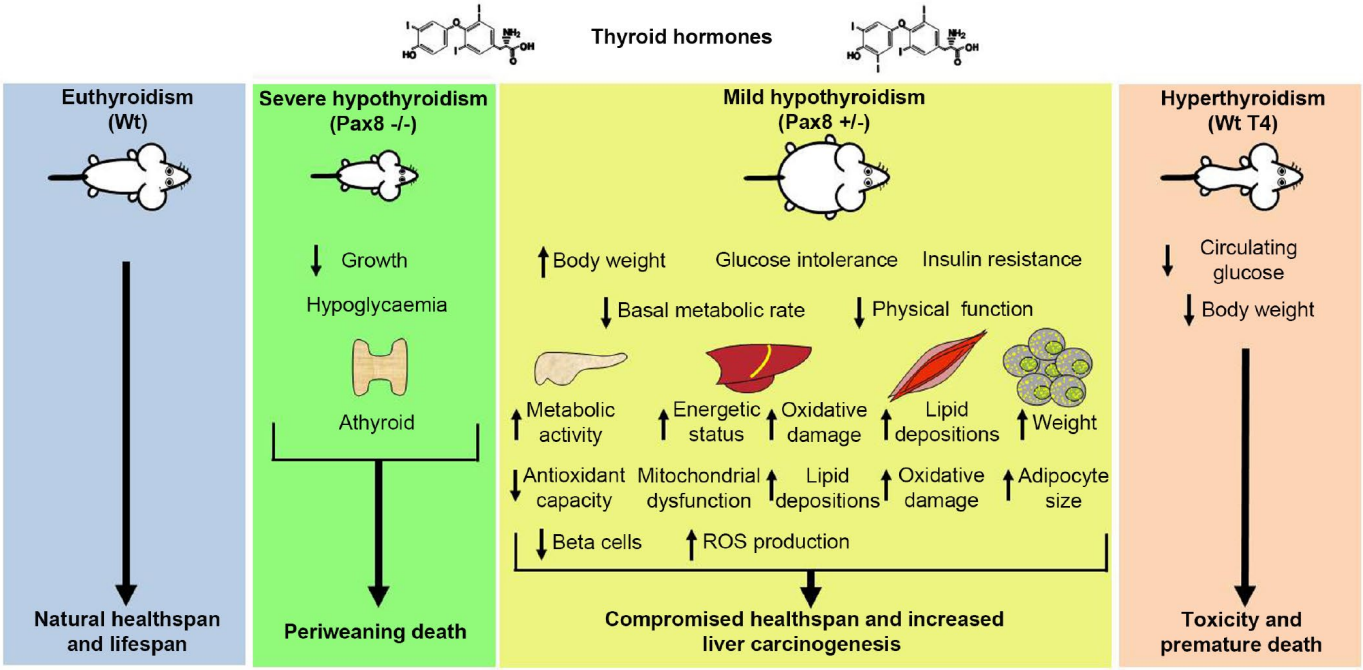

Figure 7. Schematic representation of the effects of the modulation of THs levels in healthspan and lifespan in mice. Mice unable to synthesize THs exhibit growth retardation and periweaning death. Mice exhibiting a mild reduction on circulating THs levels develop obesity, glucose metabolism dysregulations and increased incidence of liver cancers, which compromise their quality of life. Mice exhibiting increased levels of THs exhibit reduced body weight and reduced glycaemia at fasting. However, these mice develop toxicity and exhibit a short lifespan. Interventions based on the modulation of THs reduce healthspan and/or lifespan in mammals.

milieu but it is inefficient in scavenging ROS-induced damage, in a process known to be involved in carcinogenesis [57]. In line with the concept that compromised mitochondrial functionality and accumulation of oxidative damage are contributory factors to the development of most age-related diseases, our observations provide direct evidence that subtle reductions on THs, as found in humans with mild hypothyroidism, augment oxidative damage, increase the incidence of liver cancers and reduce healthspan.

In 1908 Dr. Max Rubner proposed the rate of living theory of aging and longevity, postulating that species with a low metabolic rate would have increased life expectancy when compared to species with a higher metabolic rate. In this line, restricted levels of THs, which control the metabolic rate, have been associated with increased longevity as well as metabolic fitness. Therefore, a mildly reduced thyroid axis activity has been proposed as a biomarker for healthy aging in humans [18, 21]. Here, we found that either lack of or high THs levels results in decreased lifespan and/or healthspan whereas mild reduction leads to hallmarks of NAFLD and liver cancer in mice. Our data support the notion that humans with exceptional longevity exhibiting restricted activity of the hypothalamus-pituitary-thyroid axis must have a specific genetic and/or epigenetic signature required to achieve longevity benefits [3, 6, 8]. More importantly, our data indicate that interventions based on the modulation of THs should not be targeted to increase the healthspan and lifespan in healthy mammals including humans.

METHODS

Ethics statement

Investigation has been conducted in accordance with the ethical standards and according to the Declaration of Helsinki and according to national and international guidelines and has been approved by the authors´ institutional review board.

Mice management

Procedures involving the use of live animals were approved by the CABIMER Ethical Committee of Animal Experimentation and performed in accordance with the Spanish law on animal use RD 53/2013 and the EU Directive 2010/63/EU for animal experiments. Mice (*Mus musculus*) were housed in individually ventilated cages (Tecniplast, Buguggiate, Italy) in a specific pathogen-free facility and kept under controlled environmental conditions (12 hours-light–dark cycle, 23 ± 1 °C with 30–50% relative humidity). Souralit plus 29/12 bedding (Souralit, Gerona, Spain) was sterilized by autoclave and added to each cage. Pax8 +/- mice in C57BL/6 background were obtained from Infrafrontiers mouse repository and genotyped according to previously published protocols [32, 58]. Male mice were used in all experiments reported. Mice were provided with standard rodent chow (Envigo, TD2914), unless stated otherwise, and sterilized tap water *ad libitum*. For the HFD study, a chow that provides 60 % of calories from fat was used (Envigo, TD06414) and treatment was started at 2-3 months of age. Mice were treated or not with T4 according to previously published protocols with minor modifications [35, 59, 60]. In brief, T4 treatment was started at birth (subcutaneous injections of 18 ng/g of body weight daily until weaning). After weaning, mice were supplemented with T4 in drinking water (5 µg/ml). Body weights were monitored monthly for the duration of the study. 9 month-old mice were fasted for 16 hours prior killing. 21-days old mice were not fasted prior killing.

Blinding, group size and randomization

The data analyst was blinded, whereas the operator was not blind to the group assignment of animals. Mice were selected from the pool eligible for inclusion in the study and were randomly divided into the experimental groups according to the genotype. Quantitative analysis of gene and protein expression was normalized to the mean of the control group to facilitate representation and understanding of the results. The experiments shown in Supplementary Figure 2A, 2B, 2C, 2D were normalized to glucose levels at time 0 (%) to determine whether differences in metabolic test stem from differences in basal glucose levels.

Metabolic tests

For the OGTT, mice were fasted for 6 h at 10 a.m. and received an oral dose of glucose (3 g/kg) by gavage. For the IPPTT, mice were fasted for 6 h from 10 a.m. and received an injection of sodium pyruvate (ip, 2 g/kg) by oral gavage. For the ITT, mice were fasted for 3 h from 10 a.m. and were injected with insulin (ip, 1.5 IU/kg). For the HOMA-IR, mice were fasted from 8 p.m. and glucose and insulin samples were taken at 16 hours of fasting. To determine glucose levels, blood samples were taken by venipuncture using a Precision Xceed glucometer (Abbott, Madrid, Spain). Insulin was measured in plasma using ELISA kits (Crystal Chem, Downers Grove, IL, USA).

Rotarod

Results from rotarod tests are presented as the time to fall from an accelerating rotarod (4–40 rpm over 5 minutes). Mice were given a 1-minute habituation trial

at 4 rpm on the day before the experiment. Results shown are the averages of three trials per mouse [61].

Wire hang test

For wire hang test, mice were allowed to grip a horizontal 1-mm wire with four paws up to 60 seconds and the latency to fall from the wire was determined. Three different trials were performed with each mouse [61].

MTT test

Hepatocyte metabolic activity was assessed using the Cell Proliferation Kit I (MTT) according to the manufacturer´s recommendations (Roche, Spain). Optical density was determined at 550 nm with a reference wavelength of 650 nm using a Varioskan Flash spectrophotometer (Thermo Scientific, Spain).

Transmission electron microscopy

Fresh gastrocnemius muscles were fixed overnight at room temperature in 2.5 % glutaraldehyde and 2% paraformaldehyde in 0.1 M phosphate buffer and then 72 h at 4ºC before processing for electron microscopy. Muscle samples were post-fixed with 2% osmium, rinsed, dehydrated and embedded in Durcupan resin (Fluka, Sigma-Aldrich, St. Louis, USA). To verify orientation, serial semithin sections (1.5 mm) were cut with an Ultracut UC-6 (Leica microsystems, Wetzlar, Germany) and mounted into slides and stained with 1% toluidine blue. In selected correct orientation samples, ultrathin sections (0.07 – 0.08 mm) were cut using an Ultra 45º diamond knife (Diatome Ltd, Nidau, Switzerland) and stained with lead citrate. Finally, photomicrographs were obtained under a transmission electron microscope FEI Tecnai G2 Spirit BioTwin (ThermoFisher Scientific company, Oregon, USA), using a digital camera Morada (Olympus Soft Image Solutions GmbH, Münster, Germany).

Semi-quantitative RT–PCR

Total RNA was extracted from tissue samples using the Easy-blue RNA extraction kit (Intron Biotechnology, Gyeonggi-doQiagen, Korea). Genomic DNA for mitochondrial DNA determinations, was extracted using the DNeasy Blood & tissue kit (QIAGEN, 60504), according to manufacturer's protocol. cDNA using 0.5–2 µg RNA was synthesized using SuperScript II Reverse Transcriptase (Thermo Fisher Scientific, Madrid, Spain). Real time PCR was performed on individual cDNAs or genomic DNA using SYBR green (Roche). Primer sequences are presented in Supplementary Table 4. The mRNA expression was calculated by the $2^{-\Delta\Delta CT}$ method and normalized to the expression of *Rps29*.

Western blot

Samples were lysed in radioimmunoprecipitation assay buffer (20 mM Tris–HCl (pH 7.5), 150 mM NaCl, 1 mM Na2EDTA, 1 mM EGTA, 1% NP-40, 1% sodium deoxycholate) with protease, phosphatase and deacetylase inhibitors P0044, P5725, P8340 and SC-362323. Western blots were performed according to standard methods, which involved incubation with a primary antibody of interest, followed by incubation with a horseradish peroxidase-conjugated secondary antibody and enhanced chemiluminescence (Supplementary Table 3). Blots were quantified with ImageJ, and the bands of interest were normalized to Ponceau S and/or Gapdh staining, as previously validated [62].

Islet isolation and transcriptome profiling

Pancreatic islets were isolated using a collagenase perfusion as previously described [33, 63]. cRNA preparations from murine islets were hybridized to mouse Clariom™ S Assay microarray chips, using the standard protocols of the Genomic Core Facility, CABIMER (Affymetrix, Santa CA, USA). Image analysis, quality control and quantification of data were performed using the Affymetrix GeneChip Command Console Software 4.0. Further statistic data analysis was performed using the Transcriptome Analysis Console developed by Affymetrix. Modulated pathways using Transcriptome Analysis Console software were obtained applying significantly modulated genes with a fold-change greater than 2.5. The Ingenuity Pathway Analysis platform was used to determine modulations on annotated "canonical pathways" using significantly modulated genes. Pathway pictures were generated using the annotated "canonical pathways" module of Ingenuity Pathway Analysis. Raw data are accessible at GSE123288.

Oxygen consumption and ECAR

Mitochondrial bioenergetics of primary hepatocytes cells were measured using an XF24 Extracellular Flux Analyzer (Agilent) [64]. After overnight culture cells were washed with Seahorse assay media (Seahorse Bioscience), supplemented with pyruvate at 1 mM and glutamine at 2 mM. Plates were incubated in a CO_2-free incubator at 37 °C for 1 h to allow temperature and pH equilibration, after which oxygen consumption rate (OCR) was measured in the XF24 Extracellular Flux Analyzer over a period of 88 min. Mitochondrial processes were examined through sequential injections of oligomycin (4 µM) at min 21, carbonyl cyanide 4-

(trifluoromethoxy) phenylhydrazone (FCCP; 2 μM) at min 39, rotenone (1 μM) at min 57, and antimycin A (5 μM) at min 75. ECAR was determined under basal culture conditions. At the end of the measurement, cells in each well were counted using the Scepter™ 2.0 Cell Counter to normalize the data.

Densitometry quantifications

Western blots and the area of adipocytes were quantified with ImageJ software (NIH). Quantifications of cell number/percentage were performed manually using Adobe Photoshop (Adobe).

Quantifications and statistical analyses

For comparisons between two groups, statistical significance was calculated using non-paired two-tailed student's t-test using Excel software. For other comparisons a repeated measurements two-way ANOVA test, one-way ANOVA, ANOVA on ranks or two-way ANOVA were performed using Graph Pad Prism 6 (GraphPad) or SigmaPlot 12.0 (SigmaPlot) software. A log rank statistical test was applied for survival curves (SigmaPlot). Specific statistical tests and the number of biological replicates (n) used in each panel are stated in Figure legends. Errors are represented as the standard error of the mean (SEM). For all analyses, p-value < 0.05 was considered statistically significant. Plots were designed with the software SigmaPlot 12.5 (SigmaPlot).

AUTHOR CONTRIBUTIONS

L.L.-N. and A.M.-M. performed most of the experiments. V.C.-G. performed immunohistochemical studies and analysed electron microscopy data. E.M.-F. Performed lipidomic analyses. M.S.-N. performed electron microscopy assays. M.G.-F., SY.R.-Z. and FJ.B.-S determined antioxidant activities. A.S.-C. and C.S.-O performed *in vitro* oxygen consumption assays. N.C.-V., E. M.-V., P.I.L, I. D-C, A.H., B.S. and F.M. assisted in experimentation. A.M.-M designed the study. B.R.G. and A.M.-M. supervised the study and secured funding. L.L.-N., B.R.G. and A.M.-M analysed the data and wrote the manuscript.

ACKNOWLEDGMENTS

We acknowledge the support of the pancreatic islet study group of the Spanish Association of Diabetes and the European COST Action BM1402 MouseAGE.

CONFLICTS OF INTEREST

The authors declare no conflicts of interest.

FUNDING

This work was funded by grants from the Ministerio de Economía y Competitividad, Instituto de Salud Carlos III co-funded by Fondos FEDER and from the nonprofit foundation 'Fundación Progreso y Salud' of the Andalusian Regional Ministry of Health (BFU2017-83588-P to B.R.G; CP14/00105, PI18/01590 and PI15/00134 to A.M-M; PI-0272-2017 and CD16/00118 to V.C-G; PI17/01286 to C. S-O and A. S-C).

REFERENCES

1. Brown-Borg HM. Hormonal control of aging in rodents: the somatotropic axis. Mol Cell Endocrinol. 2009; 299:64–71. https://doi.org/10.1016/j.mce.2008.07.001 PMID:18674587

2. Ooka H, Shinkai T. Effects of chronic hyperthyroidism on the lifespan of the rat. Mech Ageing Dev. 1986; 33:275–82. https://doi.org/10.1016/0047-6374(86)90052-7 PMID:3713266

3. Bowers J, Terrien J, Clerget-Froidevaux MS, Gothié JD, Rozing MP, Westendorp RG, van Heemst D, Demeneix BA. Thyroid hormone signaling and homeostasis during aging. Endocr Rev. 2013; 34:556–89. https://doi.org/10.1210/er.2012-1056 PMID:23696256

4. Solanes G, Pedraza N, Calvo V, Vidal-Puig A, Lowell BB, Villarroya F. Thyroid hormones directly activate the expression of the human and mouse uncoupling protein-3 genes through a thyroid response element in the proximal promoter region. Biochem J. 2005; 386:505–13. https://doi.org/10.1042/BJ20041073 PMID:15496137

5. Heiman ML, Tinsley FC, Mattison JA, Hauck S, Bartke A. Body composition of prolactin-, growth hormone, and thyrotropin-deficient Ames dwarf mice. Endocrine. 2003; 20:149–54. https://doi.org/10.1385/ENDO:20:1-2:149 PMID:12668880

6. Gesing A, Lewiński A, Karbownik-Lewińska M. The thyroid gland and the process of aging; what is new? Thyroid Res. 2012; 5:16. https://doi.org/10.1186/1756-6614-5-16 PMID:23176389

7. Hine C, Kim HJ, Zhu Y, Harputlugil E, Longchamp A, Matos MS, Ramadoss P, Bauerle K, Brace L, Asara JM, Ozaki CK, Cheng SY, Singha S, et al. Hypothalamic-Pituitary Axis Regulates Hydrogen Sulfide Production. Cell Metab. 2017; 25:1320–1333.e5. https://doi.org/10.1016/j.cmet.2017.05.003 PMID:28591635

8. Jansen SW, Akintola AA, Roelfsema F, van der Spoel E, Cobbaert CM, Ballieux BE, Egri P, Kvarta-Papp Z, Gereben B, Fekete C, Slagboom PE, van der Grond J, Demeneix BA, et al. Human longevity is characterised by high thyroid stimulating hormone secretion without altered energy metabolism. Sci Rep. 2015; 5:11525. https://doi.org/10.1038/srep11525 PMID:26089239

9. Flurkey K, Papaconstantinou J, Miller RA, Harrison DE. Lifespan extension and delayed immune and collagen aging in mutant mice with defects in growth hormone production. Proc Natl Acad Sci USA. 2001; 98:6736–41. https://doi.org/10.1073/pnas.111158898 PMID:11371619

10. Brown-Borg HM, Borg KE, Meliska CJ, Bartke A. Dwarf mice and the ageing process. Nature. 1996; 384:33. https://doi.org/10.1038/384033a0 PMID:8900272

11. Bartke A, Chandrashekar V, Bailey B, Zaczek D, Turyn D. Consequences of growth hormone (GH) overexpression and GH resistance. Neuropeptides. 2002; 36:201–08. https://doi.org/10.1054/npep.2002.0889 PMID:12359510

12. Brown-Borg HM. Hormonal regulation of longevity in mammals. Ageing Res Rev. 2007; 6:28–45. https://doi.org/10.1016/j.arr.2007.02.005 PMID:17360245

13. Ravussin E, Redman LM, Rochon J, Das SK, Fontana L, Kraus WE, Romashkan S, Williamson DA, Meydani SN, Villareal DT, Smith SR, Stein RI, Scott TM, et al, and CALERIE Study Group. A 2-Year Randomized Controlled Trial of Human Caloric Restriction: Feasibility and Effects on Predictors of Health Span and Longevity. J Gerontol A Biol Sci Med Sci. 2015; 70:1097–104. https://doi.org/10.1093/gerona/glv057 PMID:26187233

14. Müller MJ, Enderle J, Pourhassan M, Braun W, Eggeling B, Lagerpusch M, Glüer CC, Kehayias JJ, Kiosz D, Bosy-Westphal A. Metabolic adaptation to caloric restriction and subsequent refeeding: the Minnesota Starvation Experiment revisited. Am J Clin Nutr. 2015; 102:807–19. https://doi.org/10.3945/ajcn.115.109173 PMID:26399868

15. De Andrade PB, Neff LA, Strosova MK, Arsenijevic D, Patthey-Vuadens O, Scapozza L, Montani JP, Ruegg UT, Dulloo AG, Dorchies OM. Caloric restriction induces energy-sparing alterations in skeletal muscle contraction, fiber composition and local thyroid hormone metabolism that persist during catch-up fat upon refeeding. Front Physiol. 2015; 6:254. https://doi.org/10.3389/fphys.2015.00254 PMID:26441673

16. Giuliani C, Iezzi M, Ciolli L, Hysi A, Bucci I, Di Santo S, Rossi C, Zucchelli M, Napolitano G. Resveratrol has anti-thyroid effects both in vitro and in vivo. Food and chemical toxicology : an international journal published for the British Industrial Biological Research Association. Food Chem Toxicol. 2017; 107 (Pt A):237–247. https://doi.org/10.1016/j.fct.2017.06.044 PMID:28668442

17. Atzmon G, Barzilai N, Surks MI, Gabriely I. Genetic predisposition to elevated serum thyrotropin is associated with exceptional longevity. J Clin Endocrinol Metab. 2009; 94:4768–75. https://doi.org/10.1210/jc.2009-0808 PMID:19837933

18. Rozing MP, Westendorp RG, de Craen AJ, Frölich M, Heijmans BT, Beekman M, Wijsman C, Mooijaart SP, Blauw GJ, Slagboom PE, van Heemst D, Group LL, and Leiden Longevity Study (LLS) Group. Low serum free triiodothyronine levels mark familial longevity: the Leiden Longevity Study. J Gerontol A Biol Sci Med Sci. 2010; 65:365–68. https://doi.org/10.1093/gerona/glp200 PMID:20018826

19. Jansen SW, Roelfsema F, van der Spoel E, Akintola AA, Postmus I, Ballieux BE, Slagboom PE, Cobbaert CM, van der Grond J, Westendorp RG, Pijl H, van Heemst D. Familial Longevity Is Associated With Higher TSH Secretion and Strong TSH-fT3 Relationship. J Clin Endocrinol Metab. 2015; 100:3806–13. https://doi.org/10.1210/jc.2015-2624 PMID:26230295

20. Simonsick EM, Chia CW, Mammen JS, Egan JM, Ferrucci L. Free Thyroxine and Functional Mobility, Fitness, and Fatigue in Euthyroid Older Men and Women in the Baltimore Longitudinal Study of Aging. J Gerontol A Biol Sci Med Sci. 2016; 71:961–67. https://doi.org/10.1093/gerona/glv226 PMID:26791089

21. Rozing MP, Houwing-Duistermaat JJ, Slagboom PE, Beekman M, Frölich M, de Craen AJ, Westendorp RG, van Heemst D. Familial longevity is associated with decreased thyroid function. J Clin Endocrinol Metab. 2010; 95:4979–84. https://doi.org/10.1210/jc.2010-0875 PMID:20739380

22. Garasto S, Montesanto A, Corsonello A, Lattanzio F, Fusco S, Passarino G, Prestipino Giarritta V, Corica F. Thyroid hormones in extreme longevity. Mech Ageing Dev. 2017; 165(Pt B):98–106. https://doi.org/10.1016/j.mad.2017.03.002 PMID:28286215

23. Venditti P, Di Meo S. Thyroid hormone-induced oxidative stress. Cell Mol Life Sci. 2006; 63:414–34. https://doi.org/10.1007/s00018-005-5457-9 PMID:16389448

24. Gredilla R, Barja G, López-Torres M. Thyroid hormone-induced oxidative damage on lipids, glutathione and DNA in the mouse heart. Free Radic Res. 2001; 35:417–25. https://doi.org/10.1080/10715760100300931 PMID:11697138

25. Chi HC, Chen SL, Lin SL, Tsai CY, Chuang WY, Lin YH, Huang YH, Tsai MM, Yeh CT, Lin KH. Thyroid hormone protects hepatocytes from HBx-induced carcinogenesis by enhancing mitochondrial turnover. Oncogene. 2017; 36:5274–84. https://doi.org/10.1038/onc.2017.136 PMID:28504722

26. Barbe P, Larrouy D, Boulanger C, Chevillotte E, Viguerie N, Thalamas C, Oliva Trastoy M, Roques M, Vidal H, Langin D. Triiodothyronine-mediated up-regulation of UCP2 and UCP3 mRNA expression in human skeletal muscle without coordinated induction of mitochondrial respiratory chain genes. FASEB J. 2001; 15:13–15. https://doi.org/10.1096/fj.00-0502fje PMID:11099489

27. Lanni A, Moreno M, Lombardi A, Goglia F. Thyroid hormone and uncoupling proteins. FEBS Lett. 2003; 543:5–10. https://doi.org/10.1016/S0014-5793(03)00320-X PMID:12753895

28. He W, An X, Li L, Shao X, Li Q, Yao Q, Zhang JA. Relationship between Hypothyroidism and Non-Alcoholic Fatty Liver Disease: A Systematic Review and Meta-analysis. Front Endocrinol (Lausanne). 2017; 8:335. https://doi.org/10.3389/fendo.2017.00335 PMID:29238323

29. Gao CX, Yang B, Guo Q, Wei LH, Tian LM. High thyroid-stimulating hormone level is associated with the risk of developing atherosclerosis in subclinical hypothyroidism. Horm Metab Res. 2015; 47:220–24. https://doi.org/10.1055/s-0034-1394370 PMID:25372775

30. Chaker L, Baumgartner C, den Elzen WP, Ikram MA, Blum MR, Collet TH, Bakker SJ, Dehghan A, Drechsler C, Luben RN, Hofman A, Portegies ML, Medici M, et al, and Thyroid Studies Collaboration. Subclinical Hypothyroidism and the Risk of Stroke Events and Fatal Stroke: An Individual Participant Data Analysis. J Clin Endocrinol Metab. 2015; 100:2181–91. https://doi.org/10.1210/jc.2015-1438 PMID:25856213

31. Kovar FM, Fang IF, Perkmann T, Haslacher H, Slavka G, Födinger M, Endler G, Wagner OF. Subclinical hypothyroidism and mortality in a large Austrian cohort: a possible impact on treatment? Wien Klin Wochenschr. 2015; 127:924–30. https://doi.org/10.1007/s00508-015-0846-z PMID:26373750

32. Mansouri A, Chowdhury K, Gruss P. Follicular cells of the thyroid gland require Pax8 gene function. Nat Genet. 1998; 19:87–90. https://doi.org/10.1038/ng0598-87 PMID:9590297

33. Martin-Montalvo A, Lopez-Noriega L, Jimenez-Moreno C, Herranz A, Lorenzo PI, Cobo-Vuilleumier N, Tamayo A, Gonzalez-Guerrero C, Hofsteede J, Lebreton F, Bosco D, Toscano MG, Herranz L, et al. Transient PAX8 Expression in Islets During Pregnancy Correlates With Beta Cell Survival Revealing a Novel Candidate Gene in Gestational Diabetes Mellitus. Diabetes. 2018; 68: 109–118. https://doi.org/10.2337/db18-0285 PMID:30352879

34. Elbein SC, Das SK, Hallman DM, Hanis CL, Hasstedt SJ. Genome-wide linkage and admixture mapping of type 2 diabetes in African American families from the American Diabetes Association GENNID (Genetics of NIDDM) Study Cohort. Diabetes. 2009; 58:268–74. https://doi.org/10.2337/db08-0931 PMID:18840782

35. López-Noriega L, Cobo-Vuilleumier N, Narbona-Pérez ÁJ, Araujo-Garrido JL, Lorenzo PI, Mellado-Gil JM, Moreno JC, Gauthier BR, Martín-Montalvo A. Levothyroxine enhances glucose clearance and blunts the onset of experimental type 1 diabetes mellitus in mice. Br J Pharmacol. 2017; 174:3795–810. https://doi.org/10.1111/bph.13975 PMID:28800677

36. Gjedde S, Vestergaard ET, Gormsen LC, Riis AL, Rungby J, Møller N, Weeke J, Jørgensen JO. Serum ghrelin levels are increased in hypothyroid patients and become normalized by L-thyroxine treatment. J Clin Endocrinol Metab. 2008; 93:2277–80. https://doi.org/10.1210/jc.2007-2619 PMID:18381578

37. Malenczyk K, Szodorai E, Schnell R, Lubec G, Szabó G, Hökfelt T, Harkany T. Secretagogin protects Pdx1 from proteasomal degradation to control a transcriptional program required for β cell specification. Mol Metab. 2018; 14:108–20. https://doi.org/10.1016/j.molmet.2018.05.019 PMID:29910119

38. Sato Y, Ito T, Udaka N, Kanisawa M, Noguchi Y, Cushman SW, Satoh S. Immunohistochemical localization of facilitated-diffusion glucose transporters in rat pancreatic islets. Tissue Cell. 1996; 28:637–43. https://doi.org/10.1016/S0040-8166(96)80067-X PMID:9004533

39. Yao X, Hou S, Zhang D, Xia H, Wang YC, Jiang J, Yin H, Ying H. Regulation of fatty acid composition and lipid storage by thyroid hormone in mouse liver. Cell Biosci. 2014; 4:38. https://doi.org/10.1186/2045-3701-4-38 PMID:25105012

40. Hotamisligil GS. Inflammation and metabolic disorders. Nature. 2006; 444:860–67. https://doi.org/10.1038/nature05485 PMID:17167474

41. Mansouri A, Gattolliat CH, Asselah T. Mitochondrial Dysfunction and Signaling in Chronic Liver Diseases. Gastroenterology. 2018; 155:629–47. https://doi.org/10.1053/j.gastro.2018.06.083 PMID:30012333

42. Paradies G, Paradies V, Ruggiero FM, Petrosillo G. Oxidative stress, cardiolipin and mitochondrial dysfunction in nonalcoholic fatty liver disease. World J Gastroenterol. 2014; 20:14205–18. https://doi.org/10.3748/wjg.v20.i39.14205 PMID:25339807

43. Ma S, Yang J, Song C, Ge Z, Zhou J, Zhang G, Hu Z. Expression quantitative trait loci for PAX8 contributes to the prognosis of hepatocellular carcinoma. PLoS One. 2017; 12:e0173700. https://doi.org/10.1371/journal.pone.0173700 PMID:28339471

44. Reddy A, Dash C, Leerapun A, Mettler TA, Stadheim LM, Lazaridis KN, Roberts RO, Roberts LR. Hypothyroidism: a possible risk factor for liver cancer in patients with no known underlying cause of liver disease. Clin Gastroenterol Hepatol. 2007; 5:118–23. https://doi.org/10.1016/j.cgh.2006.07.011 PMID:17008133

45. Bano A, Dhana K, Chaker L, Kavousi M, Ikram MA, Mattace-Raso FU, Peeters RP, Franco OH. Association of Thyroid Function With Life Expectancy With and Without Cardiovascular Disease: the Rotterdam Study. JAMA Intern Med. 2017; 177:1650–57. https://doi.org/10.1001/jamainternmed.2017.4836 PMID:28975207

46. Jonklaas J, Davidson B, Bhagat S, Soldin SJ. Triiodothyronine levels in athyreotic individuals during levothyroxine therapy. JAMA. 2008; 299:769–77. https://doi.org/10.1001/jama.299.7.769 PMID:18285588

47. Lonardo A, Ballestri S, Mantovani A, Nascimbeni F, Lugari S, Targher G. Pathogenesis of hypothyroidism-induced NAFLD: Evidence for a distinct disease entity? Dig Liver Dis. 2019; 51:462–470. https://doi.org/10.1016/j.dld.2018.12.014 PMID:30733187

48. Mantovani A, Nascimbeni F, Lonardo A, Zoppini G, Bonora E, Mantzoros CS, Targher G. Association Between Primary Hypothyroidism and Nonalcoholic Fatty Liver Disease: A Systematic Review and Meta-Analysis. Thyroid. 2018; 28:1270–1284. https://doi.org/10.1089/thy.2018.0257 PMID:30084737

49. Nishi M. Diabetes mellitus and thyroid diseases. Diabetol Int. 2018; 9:108–12. https://doi.org/10.1007/s13340-018-0352-4 PMID:30603357

50. Aguayo-Mazzucato C, DiIenno A, Hollister-Lock J, Cahill C, Sharma A, Weir G, Colton C, Bonner-Weir S. MAFA and T3 Drive Maturation of Both Fetal Human Islets and Insulin-Producing Cells Differentiated From hESC. J Clin Endocrinol Metab. 2015; 100:3651–59. https://doi.org/10.1210/jc.2015-2632 PMID:26207953

51. Aguayo-Mazzucato C, Zavacki AM, Marinelarena A, Hollister-Lock J, El Khattabi I, Marsili A, Weir GC, Sharma A, Larsen PR, Bonner-Weir S. Thyroid hormone promotes postnatal rat pancreatic β-cell development and glucose-responsive insulin secretion through MAFA. Diabetes. 2013; 62:1569–80. https://doi.org/10.2337/db12-0849 PMID:23305647

52. Vinciguerra M, Carrozzino F, Peyrou M, Carlone S, Montesano R, Benelli R, Foti M. Unsaturated fatty acids promote hepatoma proliferation and progression through downregulation of the tumor suppressor PTEN. J Hepatol. 2009; 50:1132–41. https://doi.org/10.1016/j.jhep.2009.01.027 PMID:19398230

53. Palomer X, Pizarro-Delgado J, Barroso E, Vázquez-Carrera M. Palmitic and Oleic Acid: The Yin and Yang of Fatty Acids in Type 2 Diabetes Mellitus. Trends Endocrinol Metab. 2018; 29:178–90. https://doi.org/10.1016/j.tem.2017.11.009 PMID:29290500

54. Shimomura I, Shimano H, Korn BS, Bashmakov Y, Horton JD. Nuclear sterol regulatory element-binding proteins activate genes responsible for the entire program of unsaturated fatty acid biosynthesis in transgenic mouse liver. J Biol Chem. 1998; 273:35299–306. https://doi.org/10.1074/jbc.273.52.35299 PMID:9857071

55. Kim YW, Moon JS, Seo YJ, Park SY, Kim JY, Yoon JS, Lee IK, Lee HW, Won KC. Inhibition of fatty acid translocase cluster determinant 36 (CD36), stimulated by hyperglycemia, prevents glucotoxicity in INS-1 cells. Biochem Biophys Res Commun. 2012; 420:462–66. https://doi.org/10.1016/j.bbrc.2012.03.020 PMID:22430143

56. Greco D, Kotronen A, Westerbacka J, Puig O, Arkkila P, Kiviluoto T, Laitinen S, Kolak M, Fisher RM, Hamsten A, Auvinen P, Yki-Järvinen H. Gene expression in human NAFLD. Am J Physiol Gastrointest Liver Physiol. 2008; 294:G1281–87. https://doi.org/10.1152/ajpgi.00074.2008 PMID:18388185

57. Zhong H, Yin H. Role of lipid peroxidation derived 4-hydroxynonenal (4-HNE) in cancer: focusing on mitochondria. Redox Biol. 2015; 4:193–99. https://doi.org/10.1016/j.redox.2014.12.011 PMID:25598486

58. Yang D, Lai D, Huang X, Shi X, Gao Z, Huang F, Zhou X, Geng YJ. The defects in development and apoptosis of cardiomyocytes in mice lacking the transcriptional factor Pax-8. Int J Cardiol. 2012; 154:43–51. https://doi.org/10.1016/j.ijcard.2010.08.057 PMID:20851479

59. Buras A, Battle L, Landers E, Nguyen T, Vasudevan N. Thyroid hormones regulate anxiety in the male mouse. Horm Behav. 2014; 65:88–96. https://doi.org/10.1016/j.yhbeh.2013.11.008 PMID:24333846

60. Wistuba J, Mittag J, Luetjens CM, Cooper TG, Yeung CH, Nieschlag E, Bauer K. Male congenital hypothyroid Pax8-/- mice are infertile despite adequate treatment with thyroid hormone. J Endocrinol. 2007; 192:99–109. https://doi.org/10.1677/JOE-06-0054 PMID:17210747

61. Soria B, Martin-Montalvo A, Aguilera Y, Mellado-Damas N, López-Beas J, Herrera-Herrera I, López E, Barcia JA, Alvarez-Dolado M, Hmadcha A, Capilla-González V. Human Mesenchymal Stem Cells Prevent Neurological Complications of Radiotherapy. Front Cell Neurosci. 2019; 13:204. https://doi.org/10.3389/fncel.2019.00204 PMID:31156392

62. Bello RI, Alcaín FJ, Gómez-Díaz C, López-Lluch G, Navas P, Villalba JM. Hydrogen peroxide- and cell-density-regulated expression of NADH-cytochrome b5 reductase in HeLa cells. J Bioenerg Biomembr. 2003; 35:169–79. https://doi.org/10.1023/A:1023702321148 PMID:12887015

63. Jimenez-Moreno CM, Herrera-Gomez IG, Lopez-Noriega L, Lorenzo PI, Cobo-Vuilleumier N, Fuente-Martin E, Mellado-Gil JM, Parnaud G, Bosco D, Gauthier BR, Martin-Montalvo A. A Simple High Efficiency Intra-Islet Transduction Protocol Using Lentiviral Vectors. Curr Gene Ther. 2015; 15:436–46. https://doi.org/10.2174/1566523215666150630121557 PMID:26122098

64. Qiao A, Jin X, Pang J, Moskophidis D, Mivechi NF. The transcriptional regulator of the chaperone response HSF1 controls hepatic bioenergetics and protein homeostasis. J Cell Biol. 2017; 216:723–41. https://doi.org/10.1083/jcb.201607091 PMID:28183717

SUPPLEMENTARY MATERIALS

Supplementary Methods

Primary hepatocyte isolation

Primary hepatocytes were isolated from the livers of male mice as previously described [1]. In brief, livers were perfused with Hank's Balanced Salt Solution (Invitrogen) containing 5 mM glucose supplemented with 0.5 mM EGTA and 25 mM HEPES (pH 7.4 at 37°C) using a CTP100 peristaltic pump (ThermoFisher). After exsanguination of the liver, perfusion was changed to DMEM (Sigma-Aldrich D5546) supplemented with 100 U/mL Penicillin and 0.1 mg/mL Streptomycin (Pen/Strep), 15 mM HEPES, and 100 U/mL of collagenase (Type IV, Worthington). Then cells were liberated and cell suspension was then filtered through a 70 μM cell strainer and centrifuged at 50 g x 2 min 3 times. Following centrifugation, cell pellets were resuspended in DMEM (Sigma-Aldrich D5796) supplemented with Pen/Strep, 5 mM HEPES, 10 nM dexamethasone, and seeded into 24-well plates or 24-well Seahorse plates precoated with collagen I (Sigma-Aldrich). One hour later the media was changed to DMEM (Sigma-Aldrich D5546) supplemented with Pen/Strep, 5 mM HEPES, 10 nM dexamethasone and 10% FBS. Media was changed 3 h later to serum-free DMEM (Sigma-Aldrich D5546) supplemented with Pen/Strep, 5 mM HEPES, 10 nM dexamethasone and cells were cultured overnight culture for various experiments.

Rectal temperature

Rectal temperature was measured using a Temperature control unit HB 101/2 (LSI letica Scientific Instruments).

T4 and α-GSU determinations

T4 levels were determined using the total T4 enzyme immunoassay test kit (MP Biomedicals, 07BC-1007), according to the manufacturer's instructions. α-GSU levels were determined using a commercially available kit following the manufacturer's instructions (Abbexa, abx 254594) [2].

Glycated haemoglobin

HbA1c levels were determined in blood samples using Hemoglobin A1c (HbA1c) Assay kit (CrystalChem, 80099), according to the manufacturer's protocol.

Energy intake determination

In order to determine the basal daily energy intake, the total amount of chow consumed per cage was monitored weekly during 3-4 weeks. In order to determine the fasting-induced energy intake, animals were fasted overnight and the amount of chow consumed by each animal was measured after 8 hours.

Metabolic and physical activity

Mouse metabolic rate was assessed by indirect calorimetry in a 16-chamber TSE Phenomaster system (TSE Systems GmbH, Bad Homburg, Germany). Mice were housed singly with water and food available ad libitum and maintained at ~22°C under a 12:12-h light-dark cycle (light period 0700-1900). All mice were individually caged three days before the onset of the experiment for acclimation. The concentrations of oxygen and carbon dioxide were monitored at the inlet and outlet of the sealed chambers to calculate oxygen consumption. Each chamber was measured for 30 s at 30-min intervals and data were recorded for 72 h total. Locomotor activity was monitored using an infrared photocell beam grid. Food and water intake was automatically monitored using built-in sensors in each cage.

Fecal lipid content

Lipid extraction from 1 g of dried feces was performed by chloroform-methanol as previously described [3]

Transaminases determination

Got and Gpt levels were measured in blood samples using Reflotron GPT (Alanine transaminase) (Cat# 10745138) and Reflotron GOT (Aspartate transaminase) (Cat# 100745120) strips in a Reflotron Plus (Roche).

Cholesterol and triglyceride determinations

Cholesterol, HDL and low density/very low-density lipoprotein (LDL/VLDL) in serum were determined using the EnzyChrom AF HDL and LDL/VLDL Assay kit (BioAssay Systems, E2HL-100), according to manufacturer's instructions. Triglyceride levels in tissues and plasma were determined using an

EnzyChrom Triglyceride Assay Kit (BioAssay Systems, ETGA-200), according to manufacturer's instructions.

Lipidomic analyses

Lipids were extracted from approximately 20 mg of tissue using hexane-isopropanol as previously described [4] and the total lipid weight was determined gravimetrically. Total oil, measured as fatty acids, fatty acids composition and triacylglycerol (TAG) species were analyzed by GLC as previously described [5]. In brief, fatty acid methyl esters (FAMES) were obtained from isolated lipids by heating the samples at 80 °C for 1 h in 3 ml of methanol/toluene/H2SO4 (88:10:2 v/v). Heptadecanoic acid (1/10 w/w) was added to each sample as an internal standard to allow quantification. After cooling, 1 ml of heptane was added and the samples were mixed. The FAMES were recovered from the upper phase and then separated and quantified using a Hewlett–Packard 5890A gas chromatograph (Palo Alto, CA, USA) with a Supelco SP-2380 capillary column of fused silica (30 m length, 0.25 mm i.d., 0.20 µm film thickness) (Bellefonte, PA, USA). Hydrogen was used as the carrier gas, with the linear gas rate being 28 cm/s. The detector and injector temperatures were set at 220 °C and the oven was set at 170 °C, with a split ratio was 1:50. Fatty acids were identified using standards (Sigma, St. Louis, MO, USA). TAGs were separated and quantified by GLC as previously described [6] with an Agilent 6890 gas chromatograph (Palo Alto, CA, USA), and hydrogen was used as the carrier gas. Triheptadecanoic acid was added to the samples as internal standard for quantification. The injector and detector temperatures both were 380 °C, the oven temperature was 345 °C, and a head pressure gradient from 70 to 120 kPa was applied, changing this last parameter depending on the column. The gas chromatography capillary column was a J & W Scientific DB-17HT (15 m length, 0.25 mm i.d., 0.15 µm film thickness) (Folsom, CA, USA), with a linear gas rate of 50 cm/s, the split ratio was 1:80, and the detector was a flame ionization detector (FID). The different TAG molecules were identified with respect to known samples, and the FID response was corrected. Polar lipids were analyzed and quantified by HPLC. Separation by HPLC was carried out in a Waters 2695 Module (Milford, MA) equipped with a Waters 2420 ELSD. The column used was a Lichrospher 100 Diol 254-4 (5 µm; Merck) applying a method based in a linear binary gradient of solvent mixtures containing different proportions of hexane, 2-propanol, acetic acid, water and trimethylamine. The flow was 1 ml/min, data were processed using Empower software, and the ELSD was regularly calibrated using commercial high-purity standards for each lipid.

Mitochondrial complexes enzymatic activities

Complex I to III and II to III activities were measured in liver and gastrocnemius lysates by the reduction of cytochrome c in the presence of NADH or succinate, respectively, as previously described [7]. Results were expressed in nmol/mg protein/min or corrected by citrate synthase activity in the same lysates.

Mitochondrial superoxide generation

Superoxide production was determined by the reduction of partially acetylated cytochrome *c* [8]. Results were expressed in nmol/mg protein/min or corrected by citrate synthase activity in the same lysates.

Enzymatic activities

Citrate synthase activity in gastrocnemius and liver lysates was measured as previously described [7]. Results were expressed in nmol/mg protein/min.

Superoxide dismutase (Sod; E.C.1.15.1.1) activity was determined at 37 ºC using the commercial kit Ransod (Randox, UK). This method employs the xanthine/ xanthine oxidase reaction to generate superoxide radicals which react with 2-(4-iodophenyl)-3-(4-nitrophe-nol)-5-phenyl tetrazolium chloride to form a red formazan dye that absorbs at 500 nm. The superoxide dismutase activity is then measured by the degree of inhibition of this reaction. The activity of the assay is defined as the amount of Sod that inhibits the rate of formazan dye formation by 50 %. The Sod calibrator included in the kit was used. Cu–Zn-Sod activity (Sod cytosolic; Sod Cyt) was differentiated from Mn-Sod (Sod mitochondrial; Sod mit) on the basis of its sensitivity to 3 mM sodium cyanide. Results were expressed in nmol/mg protein/min.

Catalase (E.C.1.11.1.6) activity was determined by incubating samples for 1 min at 37 ºC in 66 mM phosphate buffer solution, pH 7.4, and 65 µmol H_2O_2. The reaction was stopped with 32.4 mM ammonium molybdate and the molybdate– H_2O_2 complex was measured at 405 nm. Results were expressed in nmol/mg protein/min. Glutathione reductase (Grd; E.C.1.6.4.2) activity was measured using the commercial 'Glutathione Reductase' kit (Randox, UK). Grd catalyzes the reduction of Glutathione disulfide (*e.g.* oxidized glutathione; GSSG) in the presence of NADPH, which is oxidized to $NADP^+$. Results were expressed in nmol/mg protein/min. Glutathione peroxidase (Gpx; E.C.1.11.1.9) activity was determined at 37 ºC using the commercial kit 'Ransel' (Randox, UK). Gpx catalyzes the oxidation of reduced glutathione (GSH) by cumene hydroperoxide. In the presence of Gr and NADPH, GSSG is immediately

converted to GSH with concomitant oxidation of NADPH to NADP+. The decrease in absorbance at 340 nm is measured. Results were expressed in nmol/mg protein/min. Glutathione S transferase activity (Gst; E.C.2.5.1.18) was determined in a spectrophotometer at 340 nm by measuring the formation of the conjugated of glutathione and 1-chloro-2,4-dinitrobenzene. Results were expressed in nmol/mg protein/min. NADH-Coenzyme Q oxidoreductase activity (Nqo1; EC 1.6.99.2) was measured as described [9] by following the decrease in NADH absorbance at 340 nm adapted to a Cobas Mira Autoanalyzer. The reaction mixture at a final volume of 200 µL contained 25 mM Tris·HCl (pH 7.5), 0.01% Tween 20, 0.7 mg/mL BSA (pH 7.4), 40 µM menadione, 5 µM FAD, 200 µM NADH, and tissue extract. Measurements were made at 25 s intervals over a time period of 10 min. Results were expressed in nmol/mg protein/min.

Barnes Maze

The method was performed according to a previously published protocol [10]. In brief, on the pre-training trial, mice were pre-trained to enter the escape box by guiding them to the escape box and remaining there for 2 min. The following day started the training trial (4 days). Mice were trained four trials per day and trials were separated by 15 min. Mice were free to explore the maze for 3 min or until they entered into the escape box. Once mice entered the box the buzzer was turned off and the mice were allowed to stay in the box for 1 min. The following day, subjects received a probe trial for 90 s to check the short-retention memory. During probe trial the escape box was removed. Primary latency to reach the target hole and total attempts were recorded. 7 days after the trial performed to check short-retention memory subjects received an additional the probe trial for 90 s to check long-term retention memory. Mice were not trained during the time period between probe trials.

Immunohistochemistry

Dissected tissues were fixed in 4% paraformaldehyde. Pancreatic sections (5 µm thick) were deparaffinized and rehydrated as previously described. For hematoxylin and eosin staining sections were immersed in hematoxylin (Merck) and eosin (Merck) for 4 and 2 minutes, respectively. For immunofluorescence, antigen retrieval was performed by heating in 0.01 M sodium citrate buffer (pH 6). After 1 h blocking at room temperature, sections were incubated overnight at 4°C with primary antibodies (Supplementary Table 3). Subsequently, slides were incubated with secondary antibodies (Supplementary Table 3) for 1 h at room temperature followed by DAPI-nuclear staining (Life Technologies,Carlsbad, USA).

REFERENCES

1. Zhang W, Sargis RM, Volden PA, Carmean CM, Sun XJ, Brady MJ. PCB 126 and other dioxin-like PCBs specifically suppress hepatic PEPCK expression via the aryl hydrocarbon receptor. PLoS One. 2012; 7:e37103. https://doi.org/10.1371/journal.pone.0037103 PMID:22615911

2. López-Noriega L, Cobo-Vuilleumier N, Narbona-Pérez ÁJ, Araujo-Garrido JL, Lorenzo PI, Mellado-Gil JM, Moreno JC, Gauthier BR, Martín-Montalvo A. Levothyroxine enhances glucose clearance and blunts the onset of experimental type 1 diabetes mellitus in mice. Br J Pharmacol. 2017; 174:3795–810. https://doi.org/10.1111/bph.13975 PMID:28800677

3. Kraus D, Yang Q, Kahn BB. Lipid Extraction from Mouse Feces. Bio Protoc. 2015; 5:e1375. https://doi.org/10.21769/BioProtoc.1375 PMID:27110587

4. Hara A, Radin NS. Lipid extraction of tissues with a low-toxicity solvent. Anal Biochem. 1978; 90:420–26. https://doi.org/10.1016/0003-2697(78)90046-5 PMID:727482

5. Martínez-Force E, Ruiz-López N, Garcés R. The determination of the asymmetrical stereochemical distribution of fatty acids in triacylglycerols. Anal Biochem. 2004; 334:175–82. https://doi.org/10.1016/j.ab.2004.07.019 PMID:15464966

6. Fernández-Moya V, Martínez-Force E, Garcés R. Identification of triacylglycerol species from high-saturated sunflower (Helianthus annuus) mutants. J Agric Food Chem. 2000; 48:764–69. https://doi.org/10.1021/jf9903861 PMID:10725146

7. Spinazzi M, Casarin A, Pertegato V, Salviati L, Angelini C. Assessment of mitochondrial respiratory chain enzymatic activities on tissues and cultured cells. Nat Protoc. 2012; 7:1235–46. https://doi.org/10.1038/nprot.2012.058 PMID:22653162

8. Martin-Montalvo A, Mercken EM, Mitchell SJ, Palacios HH, Mote PL, Scheibye-Knudsen M, Gomes AP, Ward TM, Minor RK, Blouin MJ, Schwab M, Pollak M, Zhang Y, et al. Metformin improves healthspan and lifespan in mice. Nat Commun. 2013; 4:2192. https://doi.org/10.1038/ncomms3192 PMID:23900241

9. Martín-Montañez E, Millon C, Boraldi F, Garcia-Guirado F, Pedraza C, Lara E, Santin LJ, Pavia J, Garcia-Fernandez M. IGF-II promotes neuroprotection and neuroplasticity recovery in a long-lasting model of

oxidative damage induced by glucocorticoids. Redox Biol. 2017; 13:69–81.
https://doi.org/10.1016/j.redox.2017.05.012
PMID:28575743

10. Patil SS, Sunyer B, Höger H, Lubec G. Evaluation of spatial memory of C57BL/6J and CD1 mice in the Barnes maze, the Multiple T-maze and in the Morris water maze. Behav Brain Res. 2009; 198:58–68.
https://doi.org/10.1016/j.bbr.2008.10.029
PMID:19022298

Supplementary Figures

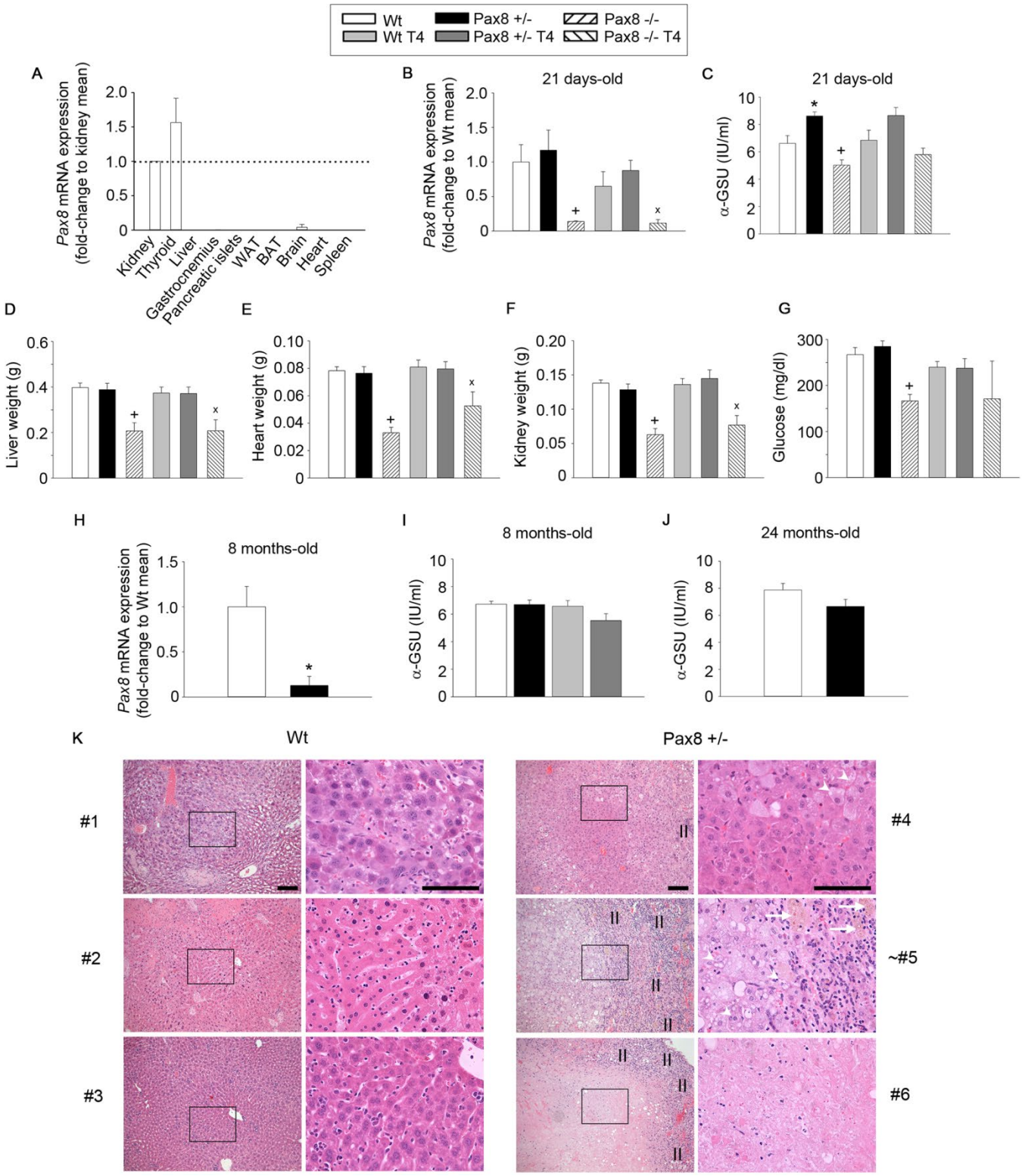

Supplementary Figure 1. Related to Figure 1. Characterization of murine models of severe hypothyroidism, mild hypothyroidism and hyperthyroidism. (**A**) Analysis of *Pax8* gene expression in different tissues in 8 month-old Wt mice. n = 3-6 kidney; n = 3 thyroid; n = 6 liver, n = 5 gastrocnemius; n = 3 pancreatic islets; n = 5 WAT; n = 6 BAT; n = 6 brain; n = 6 heart; n = 6 spleen. Reference line

indicates expression levels in kidney tissue. (**B**) Analysis of differential *Pax8* gene expression in thyroid tissue at 21 day of age. n = 7 Wt, n = 5 Pax8 +/-, n = 4 Pax8 -/-, n = 6 Wt T4, n = 5 Pax8 +/- T4, n = 4 Pax8 -/- T4. ANOVA on ranks. (**C**) Circulating α-GSU levels at 21 days of age. n = 6 Wt, n = 8 Pax8 +/-, n = 4 Pax8 -/-, n = 4 Wt T4, n = 4 Pax8 +/- T4, n = 4 Pax8 -/- T4. Two-way ANOVA. (**D**) Liver weight at 21 days of age. n = 21 Wt, n = 15 Pax8 +/-, n = 5 Pax8 -/-, n = 11 Wt T4, n = 11 Pax8 +/- T4, n = 4 Pax8 -/- T4. Two-way ANOVA. (**E**) Heart weight at 21 days of age. n = 21 Wt, n = 15 Pax8 +/-, n = 5 Pax8 -/-, n = 10 Wt T4, n = 11 Pax8 +/- T4, n = 4 Pax8 -/- T4. Two-way ANOVA. (**F**) Kidney weight at 21 days of age. n = 21 Wt, n = 14 Pax8 +/-, n = 5 Pax8 -/-, n = 11 Wt T4, n = 10 Pax8 +/- T4, n = 4 Pax8 -/- T4. Two-way ANOVA. (**G**) Blood glucose at 21 days of age. n = 14 Wt, n = 10 Pax8 +/-, n = 5 Pax8 -/-, n = 11 Wt T4, n = 11 Pax8 +/- T4, n = 4 Pax8 -/- T4. Two-way ANOVA. (**H**) Analysis of differential *Pax8* gene expression in thyroid tissue at 9 months of age. n = 3 per group. T-test two tailed. (**I**) Circulating α-GSU levels at 8 months of age. n = 7 per group. Two-way ANOVA. (**J**) Circulating α-GSU levels at 24 months of age. n = 7 per group. T-test two tailed. (**K**) Representative images of liver sections stained with hematoxylin and eosin at necropsies from Wt and Pax8+/- mice. Primary liver epithelial neoplasms were more frequently found in Pax8 +/- mice. II: inflammatory infiltrate; White arrow, cholestasis; White head arrow: steatosis. Scale bar 100 μm. #1: primary liver epithelial neoplasm. #2: normal liver. #3: normal liver. #4: primary liver epithelial neoplasm. #5: primary liver epithelial neoplasm. #6: primary liver epithelial neoplasm. n = 4 per group. Data are represented as the mean ± SEM. * p-value < 0.05 between Wt mice and Pax8 +/- mice. + p-value < 0.05 between Wt mice and Pax8 -/- mice. & p-value < 0.05 between Wt mice and Wt T4 mice. # p-value < 0.05 between Wt mice and Pax8 +/- T4 mice. x p-value < 0.05 between Wt mice and Pax8 -/- T4.

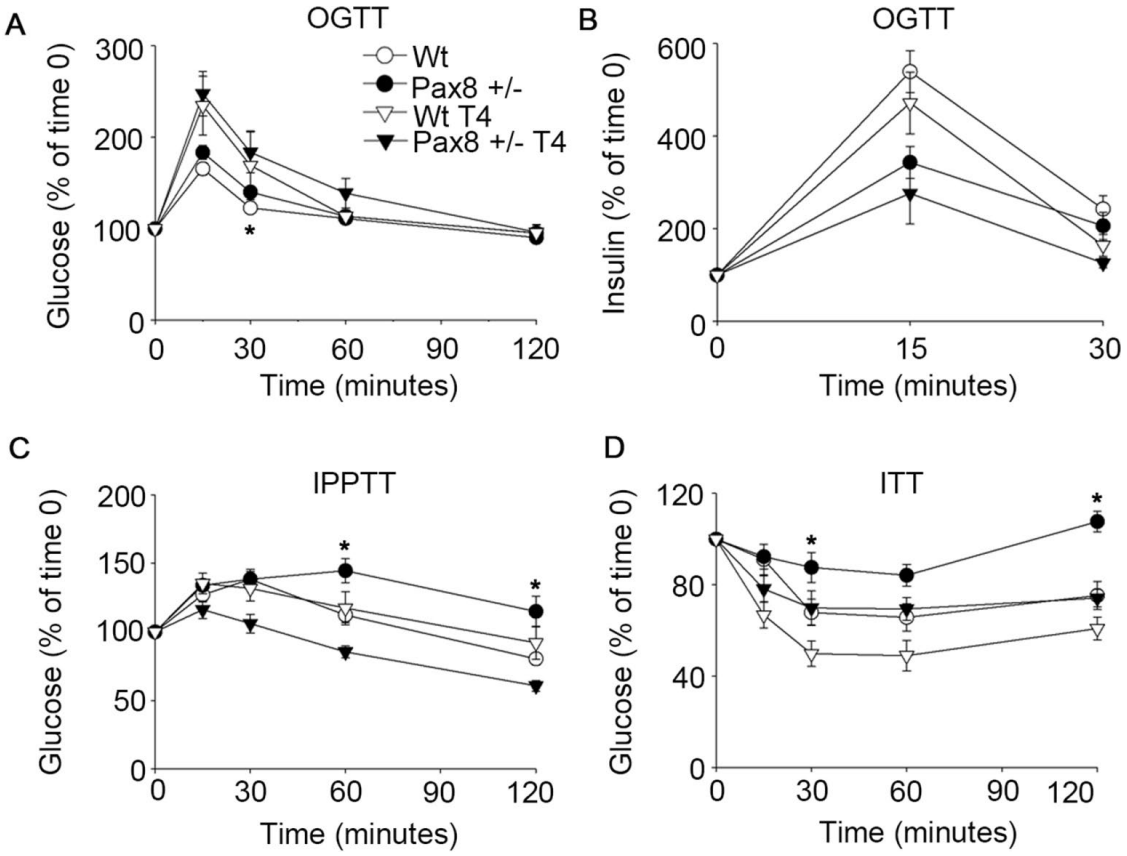

Supplementary Figure 2. Related to Figure 2. The modulation of THs alters glucose homeostasis and pancreatic islets in adulthood. (**A**) Glucose concentration in blood during the OGTT expressed as the percentage of basal glucose. n = 8 per group. (**B**) Circulating insulin during the OGTT expressed as the percentage of basal insulin. n = 8 per group. (**C**) Glucose concentration in blood during the IPPTT expressed as the percentage of basal glucose. n = 8 per group. (**D**) Glucose concentration in blood during the ITT expressed as the percentage of basal glucose. n = 8 per group. Data are represented as the mean ± SEM. * p-value < 0.05 between Wt mice and Pax8 +/- mice. & p-value < 0.05 between Wt mice and Wt T4 mice. # p-value < 0.05 between Wt mice and Pax8 +/- T4 mice. ANOVA on ranks.

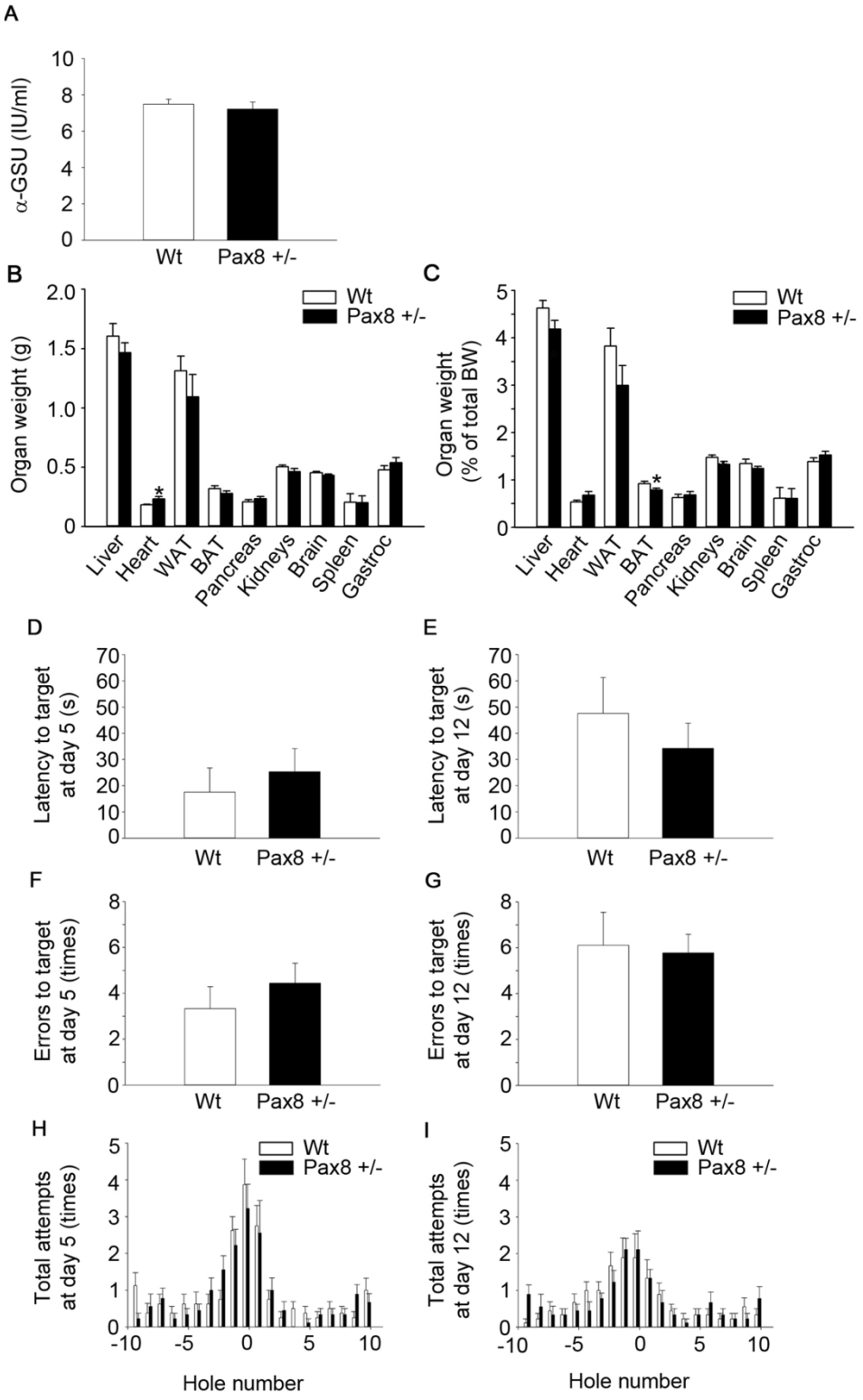

Supplementary Figure 3. Related to Figure 3. Mild hypothyroid Pax8 +/- mice fed a HFD do not exhibit major alterations on tissue weight and neurocognitive function. (**A**) Circulating α-GSU levels at 7 months of life. n = 7 Wt, n = 4 Pax8 +/-. (**B**) Tissues weight at sacrifice (9 months-old). n = 9 per group. (**C**) Tissues weight corrected by total body weight at sacrifice (9 months-old). n = 9 per group. (**D**) Latency to target at day 5 in Barnes maze. n = 9 per group. (**E**) Latency to target at day 12 in Barnes maze. n = 9 per group. (**F**) Errors to target at day 5 in Barnes maze. n = 9 per group. (**G**) Errors to target at day 12 in Barnes maze. n = 9 per group. (**H**) Total attempts to target in Barnes maze at day 5. n = 9 per group. (**I**) Total attempts to target in Barnes maze at day 12. n = 9 per group. Data are represented as the mean ± SEM. Barnes Maze experiments were performed at week 19-20 of HFD feeding (8 month–old). * p-value < 0.05. T-test two tailed.

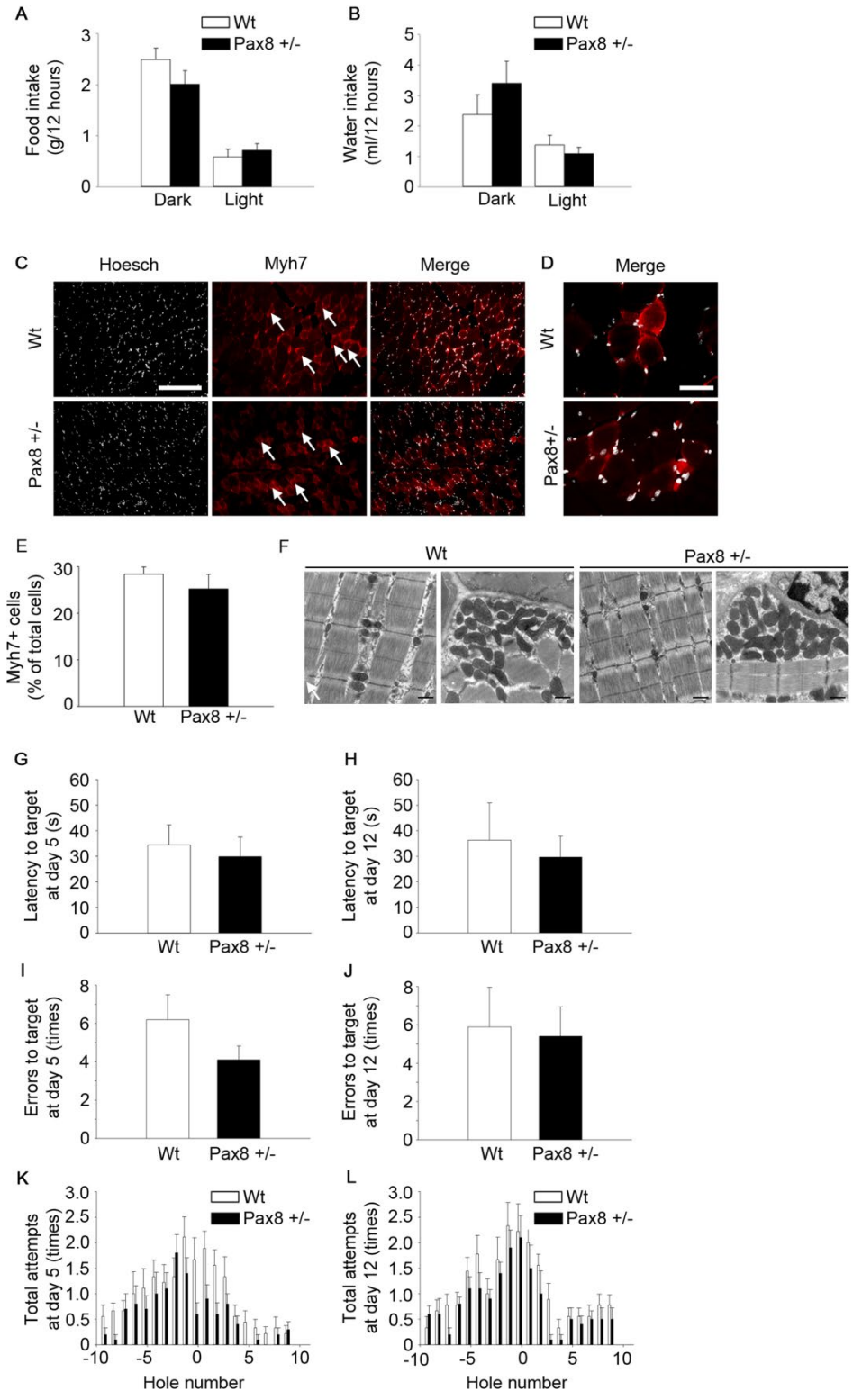

Supplementary Figure 4. Related to Figure 4. Mild hypothyroid Pax8 +/- mice fed a STD do not exhibit alterations food intake, water intake and neurocognitive function. (**A**) Energy intake determined during indirect calorimetry experiments. n = 8 Wt, n = 7 Pax8 +/-. (**B**) Water consumption determined during indirect calorimetry experiments. n = 8 Wt, n = 7 Pax8 +/-. (**C**) Myh7 immunostaining of gastrocnemius sections. Representative Myh7 expressing myofibers are marked with arrows. n = 6 per group. Scale bar: 250 µm. (**D**) Magnifications of Myh7 positive myofibers of gastrocnemius sections. n = 6 per group. Scale bar: 50 µm. (**E**) Quantification of the percentage of Myh7 expressing myofibers in the gastrocnemii. n = 6 per group. (**F**) Representative transmission electron microscopy images of gastrocnemius sections. n = 6 per group. Scale bar: 500 nm. (**G**) Latency to target at day 5 in Barnes maze. n = 10 per group. (**H**) Latency to

target at day 12 in Barnes maze. n = 10 per group. (**I**) Errors to target at day 5 in Barnes maze. n = 10 per group. (**J**) Errors to target at day 12 in Barnes maze. n = 10 per group. (**K**) Total attempts to target in Barnes maze at day 5. n = 10 per group. (**L**) Total attempts to target in Barnes maze at day 12. n = 10 per group. Mice were 7 month-old in indirect calorimetry experiments. Mice were 8 month-old in Barnes Maze experiments. Mice were 9 month-old at the time of killing. Data are represented as the mean ± SEM. * p-value < 0.05. T-test two tailed.

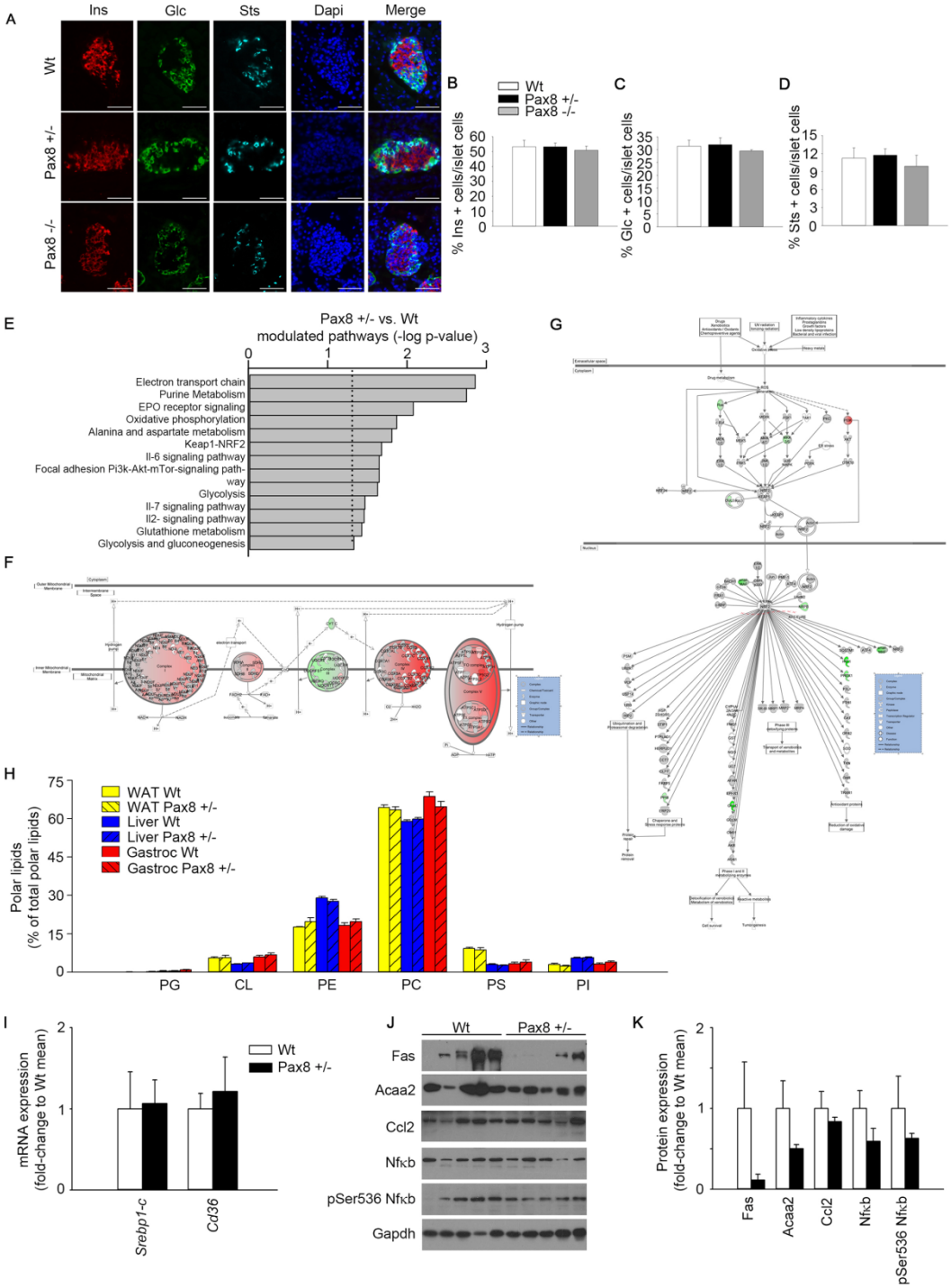

Supplementary Figure 5. Related to Figure 5. Mild hypothyroid Pax8 +/- mice exhibit metabolic alterations in metabolic tissues. (**A**) Representative immunofluorescence images of pancreatic sections from untreated Wt, Pax8 +/- and Pax8 -/- male mice at postnatal day 21. Scale bar: 50 µm. n = 4 per group. (**B**) Percentage of insulin positive cells in islet cells at postnatal day 21. n = 4 per group. One-way ANOVA. (**C**) Percentage of glucagon positive cells in islet cells at postnatal day 21. n = 4 per group. One-way ANOVA. (**D**) Percentage of somatostatin positive cells in islet cells at postnatal day 21. n = 4 per group One-way ANOVA. (**E**) Analysis of significantly modulated

pathways in pancreatic islets using Transcription Analysis Console platform. n = 3 per group. Statistical analysis was performed using Transcription Analysis Console using significantly modulated genes with a fold change ≥ 2.5 or a fold change ≤-2.5. (**F**) Representative picture of the annotated canonical pathway "oxidative phosphorylation" generated by Ingenuity Pathway Analysis platform. (**G**) Representative picture of the annotated canonical pathway "NRF2-mediated oxidative stress response" generated by Ingenuity Pathway Analysis platform. (**H**) Lipidomic analysis depicting percentages of the different species of polar lipids in WAT, liver and gastrocnemius. PG: Phosphatidylglycerol. CL: Cardiolipin. PE: Phosphatidylethanolamine. PC: Phosphatidylcholine PS: Phosphatidylserine PI: Phosphatidylinositol. n = 5 Wt, n = 6 Pax8 +/-. Two-way ANOVA. (**I**) mRNA expression of genes involved in lipid synthesis/import in gastrocnemius. *Srebp1-c*: n = 6 Wt, n = 5 Pax8 +/-; *Cd36*: n = 5 Wt, n = 6 Pax8 +/-. T-test two tailed. (**J**) Western blots showing proteins involved in lipogenesis in gastrocnemius lysates. n = 5 per group. (**K**) Densitometric analysis of western blots shown in panel J. T-test two tailed. Data are represented as the mean ± SEM. Ins: insulin. Glc: glucagon. Sts: somatostatin. Unless otherwise stated, mice were 9 month-old at the time of killing. * p-value < 0.05.

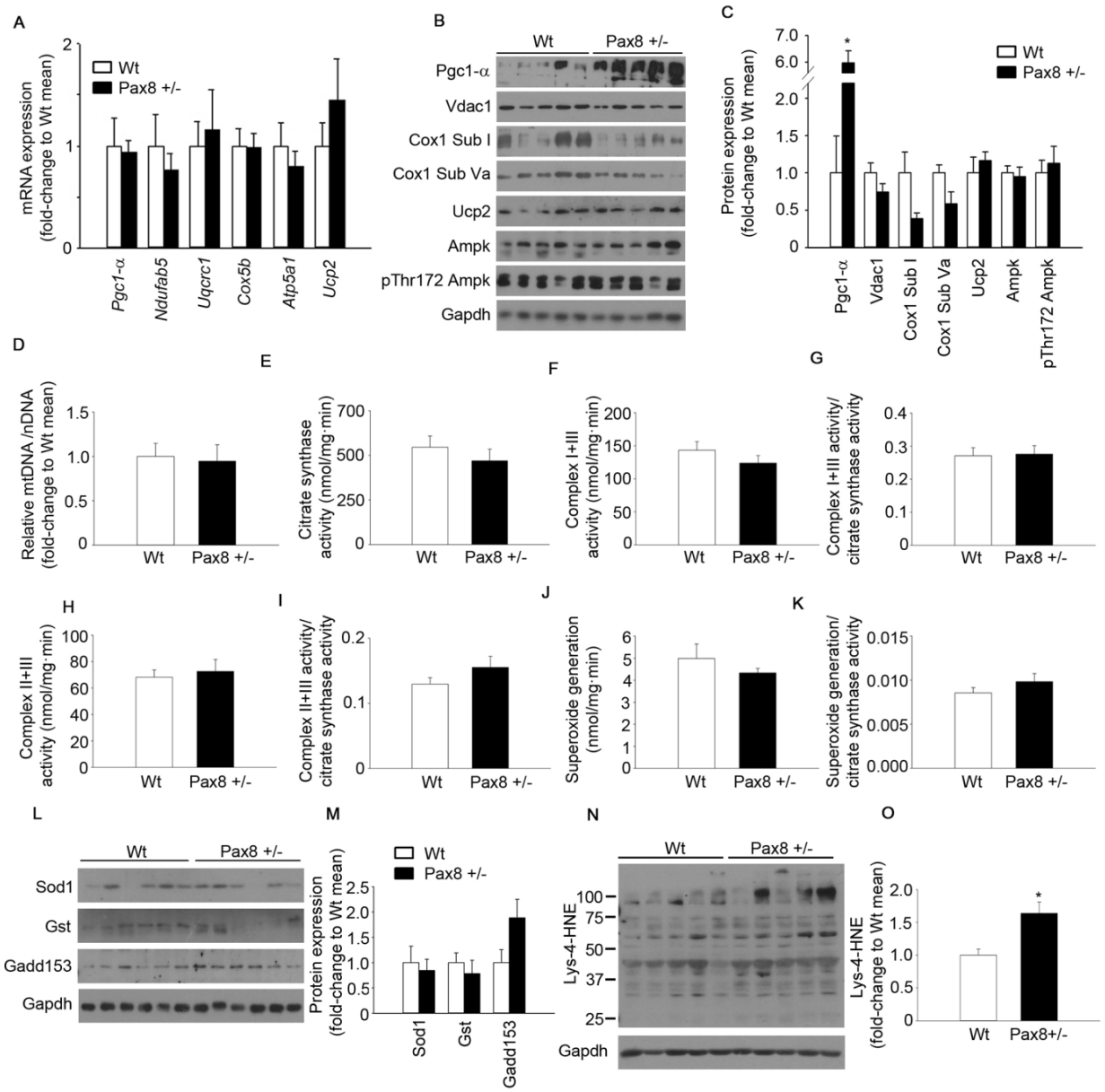

Supplementary Figure 6. Related to Figure 6. Mild hypothyroidism increases the accumulation of oxidative damage in the gastrocnemius. (**A**) mRNA expression of genes involved in mitochondrial biogenesis and function in the gastrocnemii. *Pgc1-α*: n = 5 Wt, n = 4 Pax8 +/-. *Ndufab5*: n = 5 Wt, n = 4 Pax8 +/-. *Uqcrc1*: n = 6 Wt, n = 5; Pax8 +/-. *Cox5b*: n = 5 Wt, n = 4 Pax8 +/-. *Atp5a1*: n = 5 Wt, n = 4 Pax8 +/-. *Ucp2*: n = 5 per group. (**B**) Western blots showing proteins involved in mitochondrial biogenesis/function as well as Ampk and its phosphorylated isoform in gastrocnemius lysates. n = 5 per group. (**C**) Densitometric analysis of western blots shown in panel B. n = 5 per group. (**D**) Relative mitochondrial DNA content in gastrocnemius isolations. n = 6 per group. (**E**) Citrate synthase activity in gastrocnemius

extracts. n = 6 per group. (**F**) Complex I+III activity in gastrocnemius extracts. n = 6 per group. (**G**) Complex I+III activity corrected by citrate synthase activity in gastrocnemius extracts. n = 6 per group. (**H**) Complex II+III activity in gastrocnemius extracts. n = 6 per group. (**I**) Complex II+III activity corrected by citrate synthase activity in gastrocnemius extracts. n = 6 per group. (**J**) Superoxide generation in mitochondrial complexes in gastrocnemius extracts. n = 5 Wt, n = 6 Pax8 +/-. (**K**) Superoxide generation in mitochondrial complexes corrected by citrate synthase activity in gastrocnemius extracts. n = 5 Wt, n = 6 Pax8 +/-. (**L**) Western blots showing expression levels of antioxidant and stress response proteins in gastrocnemius lysates. n = 6 per group. (**M**) Densitometric analysis of the western blot shown in panel L. (**N**) Western blot showing Lys-4-HNE staining in gastrocnemius extracts. n = 5 per group. (**O**) Densitometric analysis of western blots shown in panel N. Mice were 9 month-old at the time of killing. Data are represented as the mean ± SEM. * p-value < 0.05. T-test two tailed.

Supplementary Tables

Supplementary Table 1. Major gross pathologies identified at necropsy.

Tissue	Pathology	Wt (52/ %)	Wt T4 (14/ %)	Pax8 +/- (17/ %)	Pax8 +/- T4 (18/ %)	Pax8 -/- (8/ %)	Pax8 -/- T4 (5/%)
Heart	Enlarged	4/ 8%	1/ 7%	1/ 7%	4/ 22%	0/ 0%	0/ 0%
Kidney	Necrotic	4/ 8%	0/ 0%	1/ 7%	0/ 0%	0/ 0%	0/ 0%
Liver	Cancer	9/ 17%	0/ 0%	8/ 47%*	0/ 0%	0/ 0%	0/ 0%
	Enlarged	14/ 27%	0/ 0%	9/ 53%	2/ 11%	0/ 0%	0/ 0%
Spleen	Enlarged	9/ 17%	0/ 0%	7/ 41%	3/ 17%	0/ 0%	0/ 0%

The percentage of mice presenting with various pathologies is represented. * $p < 0.05$ compared to Wt. Analysed using Fisher's Exact Test.

Supplementary Table 2. List of the most modulated transcripts in pancreatic islets isolated from Pax8 +/- and Wt mice.

Gene Symbol	Fold Change	p-value
Scgn	30.08	0.0253
Gm11096	28.36	0.0035
Pcsk1n	15.77	0.0450
Slc2a5	12.74	0.0440
Mlxipl	12.64	0.0461
Wdr83os	12.49	0.0310
Abat	12.43	0.0202
Slc25a42	11.52	0.0277
Insrr	11.46	0.0420
Cfap126	11.24	0.0204
Serpini2	−10.51	0.0278
Galnt3	−10.7	0.0335
Ero1l	−10.99	0.0183
Tm4sf1	−13.3	0.0471
Igfbp3	−16.46	0.0464
Ak4	−21.78	0.0363
Hmox1	−24.1	0.0341
Reg2	−29.21	0.0465
Pfkfb3	−31.12	0.0393
Slc2a1	−42.5	0.0461

Supplementary Table 3. Antibodies used in this study.

Antibody	Dilution	Vendor	Catalog number
Alexa fluor 647 donkey anti-mouse	1:800	Thermofisher	Cat# A-31571, RRID:AB_162542):
Alexa fluor 555 donkey anti-rabbit	1:800	Thermofisher	Cat# A-31572, RRID:AB_162543
Alexa fluor 488 donkey anti-goat	1:800	Thermofisher	Cat# A-11055, RRID:AB_2534102
Anti-insulin	1:500	Sigma-Aldrich	Cat# I2018, RRID:AB_260137
Anti-insulin	1:500	Santa Cruz Biotechnology	Cat# sc-9168, RRID:AB_2126540
Anti-glucagon	1:150	Cell Signaling	Cat# 2760, RRID:AB_659831
Anti-glucagon	1:100	Sigma-Aldrich	Cat# G2654, RRID:AB_259852
Anti-somatostatin	1:150	Santa Cruz Biotechnology	Cat# sc-7819, RRID:AB_2302603
Anti-pSer473 Akt	1:500	Cell Signaling	Cat# 9271, RRID:AB_329825
Anti-Akt	1:1000	Cell Signaling	Cat# 9272, RRID:AB_329827
Anti-Gapdh	1:1000	Cell Signaling	Cat# 2118, RRID:AB_561053
Anti-pThr172 Ampk	1:1000	Cell Signaling	Cat# 2535, RRID:AB_331250
Anti-Ampk	1:1000	Cell Signaling	Cat# 2532, RRID:AB_330331
Anti-Lc3b	1:1000	Cell Signaling	Cat# 2775, RRID:AB_915950)
Anti-Ucp2	1:200	Santa Cruz Biotechnology	Cat# sc-6526, RRID:AB_2213582
Anti-Vdac1	1:1000	Abcam	Cat# ab15895, RRID:AB_2214787
Anti-Pgc1-α	1:1000	Santa Cruz Biotechnology	Cat# sc-517380, RRID:AB_2755043
Anti- cytochrome *c* oxidase subunit Va	1:1000	Molecular probes	Cat# A21363, RRID:AB_1501848
Anti- cytochrome *c* oxidase subunit I	1:1000	Molecular probes	Cat# A-6403, RRID:AB_221582
Anti-4hne	1:1000	Millipore	Cat# 393206-100UL, RRID:AB_211975
Anti-Fas	1:200	Santa Cruz Biotechnology	Cat# sc-55580, RRID:AB_2231427
Anti-Acaa2	1:200	Santa Cruz Biotechnology	Cat# sc-100847, RRID:AB_2219392
Anti-Ccl2	1:200	ENZO	Cat# ALX-804-549-C100, RRID:AB_2050978
Anti-NfκB	1:1000	Abcam	Cat# ab32536, RRID:AB_776751
Anti-pSer536 NfκB	1:1000	Cell Signaling	Cat# 3033, RRID:AB_331284
Anti-Sod1	1:2000	Abcam	Cat# ab13498, RRID:AB_300402
Anti-Gst	1:1000	Sigma-Aldrich	Cat# G1160, RRID:AB_259845
Anti-Gadd153	1:200	Santa Cruz Biotechnology	Cat# sc-575, RRID:AB_631365
Anti-Myh7	1:150	Santa Cruz Biotechnology	Cat# sc-53090, RRID:AB_2147279
HRP-goat anti-rabbit	1:5000	Sigma-Aldrich	Cat# A0545, RRID:AB_257896
HRP-rabbit anti-mouse	1:5000	Sigma-Aldrich	Cat# A9044, RRID:AB_258431
HRP-IgGκ light chain binding protein anti-mouse	1:1000	Santa Cruz Biotechnology	Cat# sc-516102, RRID:AB_2687626
HRP-donkey anti-goat	1:2000	Jackson ImmunoResearch Labs	Cat# 705-036-147, RRID:AB_2340392

Supplementary Table 4. Primers used for RT-PCR in this study.

Gene	Forward primer sequence	Reverse primer sequence
Mouse mtNd1	5′–CCTATCACCCTTGCCATCAT–3′	5′–GAGGCTGTTGCTTGTGTGAC–3′
Mouse nPecam	5′–ATGGAAAGCCTGCCATCATG–3′	5′–TCCTTGTTGTTCAGCATCAC–3′
Mouse Pgc1-α	5′–GGGTCAGAGGAAGAGATAAAGTTG–3′	5′–CACCAAACCCACAGAAAACAG–3′
Mouse Pax8	5′–GTTTGAGCGGCAGCATTAC–3′	5′–GTAAGGGCAGTGGGTACAGC–3′
Mouse Rps29	5′-GGAGTCACCCACGGAAGTT-3′	5′-CATGTTCAGCCCGTATTTGC-3′
Mouse Ucp2	5′-GCTTGGGATCCTGGAACGT-3′	5′-GGCAGCCATTAGGGCTCTTT-3′
Mouse Srebp1-c	5′-GCATGCCATGGGCAAGTAC-3′	5′–AGCATCTCCTGCGCACTCA–3′
Mouse Srebp2	5′- ACCGGTCCTCCATCAACG-3′	5′- CCAGGTCGATGCCCTTCA-3′
Mouse Fasn	5′-TCCTGAATCAGCCCACG-3′	5′-ACACCCATGAGCGAGTCC-3′
Mouse Cd36	5′-CACAGACGCAGCCTCCTT-3′	5′-TGGATTCTGGAGGGGTGA-3′
Mouse Socs2	5′-GTAAGGGCAGTGGGTACAGC-3′	5′-GGTAAAGGGAGTCCCCAGA-3′
Mouse Il-1β	5′-AACTGTTGGTGAGGAATGTGG-3′	5′-GGTCCTGTCCCTCTTGTTTTCA-3′
Mouse Tnf-α	5′-CCCTCACACTCAGATCATCTTCT-3′	5′-GCTACGACGTGGGCTACAG-3′
Mouse Cpt1	5′-AGACAAGAACCCCAACATCC-3′	5′-CAAAGGTGTCAAATGGGAAGG-3′
Mouse Lcad	5′-GGTGGAAAACGGAATGAAAGG-3′	5′-GGCAATCGGACATCTTCAAG-3′
Mouse Mcad	5′-TGTTAATCGGTGAAGGAGCAG-3′	5′-CTATCCAGGGCATACTTCGTG-3′
Mouse Atp5a1	5′-CATTGGTGATGGTATTGCGC-3′	5′-TCCCAAACACGACAACTCC-3′
Mouse Cox5b	5′-ACCCTAATCTAGTCCCGTCC-3′	5′–CAGCCAAAACCAGATGACAG–3′
Mouse Uqcrc1	5′-ATCAAGGCACTGTCCAAGG-3′	5′-TCATTTTCCTGCATCTCCCG-3′
Mouse Ndufab5	5′-GGACCGAGTTCTGTATGTCTTG-3′	5′-AAACCCAAATTCGTCTTCCATG-3′
Mouse Cish	5′–GCATAGCCAAGACGTTCTCC–3′	5′–AATGTACCCTCCGGCATCTT–3′